NASA

Technical Memorandum 85090

THE ROLE OF SATELLITE-MEASURED EQUIVALENT BLACKBODY TEMPERATURE IN THE STUDY OF ATLANTIC OCEAN TROPICAL CYCLONES

Joseph Steranka
Edward B. Rodgers
R. Cecil Gentry

AUGUST 1983

National Aeronautics and
Space Administration

Goddard Space Flight Center
Greenbelt, Maryland 20771

TM 85090

THE ROLE OF SATELLITE-MEASURED EQUIVALENT BLACKBODY TEMPERATURE IN THE STUDY OF ATLANTIC OCEAN TROPICAL CYCLONES

Joseph Steranka
General Software Corporation,
Landover, MD 20785

Edward B. Rodgers
Goddard Laboratory for Atmospheric Sciences
NASA Goddard Space Flight Center
Greenbelt, MD 20771

R. Cecil Gentry
Department of Physics and Astronomy,
Clemson University,
Clemson, SC 29631

August 1983

GODDARD SPACE FLIGHT CENTER
Greenbelt, Maryland

1. INTRODUCTION

The meteorological satellite is providing highly useful information which is applied operationally each day in the interpretation of weather conditions. The polar orbiting satellite provides a complete view of the earth twice daily with even more frequent observations at high latitudes because of overlapping fields of view in the successive orbits. The geosynchronous satellite with its high temporal resolution provides observations each 30 minutes or less. The ability to monitor the more isolated regions of the earth with the satellite has proved to be particularly useful for tropical latitudes where only few meteorological stations view the broad ocean expanses. With the satellite, the disruption of the normally quiescent tropical weather is readily observed. As tropical cyclones develop, the information obtained with such monitoring becomes the basis for many of the warnings and for predictions of the storm's track and intensity.

The satellite views the cloud tops, as well as the exposed earth's surface, and information about the atmosphere's dynamics and kinematics gained from this source is limited to inferences made from measurements of the cloud motion, cloud top temperature, and an analysis of cloud character and distribution. Investigators have shown that such inferences are highly useful in describing the state of the atmosphere and in explaining its behavior. Cloud motion measurements obtained from sequential satellite imagery were used to make quantitative

intensity assessments of the tropical cyclone (Fujita and Tecson, 1974[1]; Erickson, 1974[2]; Smith, 1975; Hawkins, 1976[3]; Rodgers, et al., 1979). Other intensity assessments were made using the upper tropospheric temperature anomalies derived from measurements made with the Nimbus 6 Scanning Microwave Spectrometer (SCAMS) (Kidder, et al., 1978). These anomalies are used in developing estimates of the minimum central sea level pressure of a storm through hydrostatic considerations.

Other investigators found that certain parameters derived from satellite measurements are related to future tropical cyclone intensity. Cloud motion measurements were used to describe the upper tropospheric asymmetry of the tropical cyclone (Black and Anthes, 1971). The asymmetry is related to future intensity through energy flux and momentum. Cloud top temperature measurements of tropical cyclones obtained with the Temperature Humidity Infrared Radiometer (THIR) window channel (11.5 μm) were used to predict storm intensification (Gentry, et al., 1980). The magnitude and distribution of the deep convection inferred from the equivalent blackbody temperature measurements serve as an index of the latent heat energy available for conversion to kinetic energy. Latent heat release of eastern Pacific Ocean tropical cyclones

---

[1]Fujita, T.T., and J.J. Tecson, 1974: A kinematic analysis of tropical storm based on ATS cloud motion. SMRP Research Paper #125, The University of Chicago, 20 pp.

[2]Erickson, C.O., 1974: Use of geostationary satellite cloud vectors to estimate tropical cyclone intensity. NOAA Tech. Memo. NESS 59, 37 pp.

[3]Hawkins, H.F., 1976: A brief comparison of some of the conditions attending hurricane Carmen and Fifi (1974). NOAA Tech. Memo., ERL WMPO-31, 8 pp.

has also been inferred from passive microwave measurements obtained with the Electrically Scanning Microwave Radiometer (ESMR) of Nimbus 5 (Adler and Rodgers, 1977; Rodgers and Adler, 1981) and found to be related to future intensity changes. Environmental wind fields developed from short-interval satellite images were used to develop local change of net relative angular momentum, areal mean relative vorticity, and upper tropospheric horizontal divergence in the study of storm intensification (Rodgers and Gentry, 1983).

The diurnal variation of cloudiness of tropical cyclones was investigated using a densitometer to measure the areal distribution of cloud tops shown with geosynchronous satellite imagery (Browner, et al., 1977). Morning-to-evening cloudiness changes over tropical oceans were studied with the radiance measurements in the water vapor window (10.5-12.5 μm) of polar orbiting NOAA satellites (Short and Wallace, 1980).

The results of the research efforts are promising but only few of the studies have produced techniques which are sufficiently developed to be used in the operational prediction of tropical cyclones. Largely because of this, the operational application of satellite information is constrained and still mostly limited to qualitative judgments where cloud character and distribution are used to assess the present intensity and to predict future intensity (Dvorak, 1975). Operational needs are best met with quantitative measurements which can be used objectively and readily obtained. Few objective measurements are as readily obtained as the equivalent blackbody temperature (T_{BB}). This report will demonstrate the utility of the high temporal resolution T_{BB} measurements made with the geosynchronous satellite in diagnosing the state of the tropical cyclone and in predicting its future intensity.

2. DATA

The data used in this study consists of T_{BB} measurements and maximum winds of Atlantic Ocean tropical cyclones. The dependent data set is comprised of 444 observations of 17 tropical cyclones occurring during 1974-1977. The independent data set consists of 94 observations of 6 tropical cyclones which occurred during 1976-1979.

The T_{BB} was measured with the infrared channel (11.5 μm) of the Visible and Infrared Spin Scan Radiometer (VISSR) of the Synchronous Meteorological Satellite (SMS) and Geostationary Operational Environmental Satellite (GOES). The maximum winds are from the best track record of the tropical cyclones compiled by the National Hurricane Research Center.

The T_{BB} data were tabulated from measurements made at 3 hr intervals of the clouds and the exposed earth's surface at and surrounding the tropical cyclone. The data compilation for each individual observation was made using the Atmospheric and Oceanographic Information Processing System (AOIPS) at Goddard Space Flight Center. The mean T_{BB} was obtained for each concentric ring (annulus) at 111 km (1° lat) intervals around the tropical cyclone center outward to 888 km. In Fig. 1, a grid is superimposed upon a satellite image of hurricane Ella. The grid is centered at the center of the hurricane. The hurricane center was readily located when there was a visible eye; in other instances, the images were aligned (Lagrangian transformation), then looped in sequence so that the center could be defined. The mean

T_{BB} for each ring contains measurements of the cloud top as well as any of the exposed earth's surface. The clouds within any data ring may consist of cirriform tops, convective towers, mid-level or low level tops.

The T_{BB} measurements obtained with the SMS and GOES were found to compare favorably within coincidental geographic areas and with sea surface temperatures in clear sky regions. At the low (cold) end of the T_{BB} measurement range no independent measurements were available for comparison and measurements were accepted whenever the T_{BB} values were $\geq$ 190 K, providing that the upper (warm) end of the range was also acceptable.

3. DIAGNOSTIC RESULTS

The T_{BB} provides a measure of the strength of the inner core convection of a tropical cyclone and further information on the distribution of the associated spreading cloudiness. At the tropical cyclones inner core, where warm moist air ascends in cumulus towers to reach the tropopause, the magnitude of the mean T_{BB} serves as an index of latent heat release and is useful in predicting storm intensity (Gentry, et al., 1980). Further removed from the center the mean T_{BB} helps to describe the spreading of upper level clouds. Beyond the storm's circulation the mean T_{BB} is used to describe the organization of clouds and clear regions.

a. *Diurnal variation of tropical cyclone cloudiness.*

The composited hourly mean T_{BB} from the tropical cyclone study set exhibit a pattern of diurnal changes which tend to affect all storms. The composited data are stratified to show the mean T_{BB} distribution as a function of distance and time and are grouped into tropical storm and hurricane intensity categories (Figs. 2 and 3 respectively). Both the dependent and independent data sets were used for the composites. The T_{BB} data consist only of observations taken where the tropical cyclone center was $\geq$111 km from a land mass. To aid in the interpretation of the diurnal changes which are apparent in the diurnal mean T_{BB} curves, a Fourier analysis of the time series was made and the first and second harmonics are shown in Figs. 4 and 5. Additionally, Tables 1 and 2 provide amplifying statistical information.

Considering that from the mean T_{BB} an inference of cloud distribution can be made, the curves shown in Figs. 2 and 3 represent a measure of the clouds which exist in and around the tropical cyclone and define the diurnal cloud cycle.

Tropical storm diurnal variation. Within the tropical storm (Fig. 2) the most evident features are:

1) a diurnal cloud maximum (minimum T_{BB}) occurs at 0700 LST and a minimum (maximum T_{BB}) at 1900 LST at the inner core (55.5 km).
2) a semidiurnal cloud oscillation exists outside the storm's circulation (499.5-832.5 km) with cloud maxima near 0600 and 1800 LST and minima near 0100 and 1000 LST.
3) a mixed pattern of cloudiness exists at the intermediate radii (166.5 to 388.5 km) (these radii include part of the storm circulation as well as the immediately adjacent environment).
4) a maximum cloud variation exists at the intermediate radii.
5) the highest clouds (coldest T_{BB}) are located nearest to the storm center (55.5 km).
6) the strongest mean T_{BB} gradient (greatest change in cloud top height) occurs between 55.5 and 277.5 km.

The periodicity of these events is better illustrated with the Fourier analysis of the time series. The curves of the first and second harmonics of the diurnal mean T_{BB} curves are shown in Fig. 4 and

Table 1. Statistics of the Fourier analysis of the diurnal time series of the mean T_{BB} distribution of Atlantic Ocean tropical storms.

1	2	3	4	5	6	7		8	9	10
55.5	221.5	2.28	1937	2.73	0.72	0857	2057	0.60	0.04	12000
166.5	240.7	2.07	2125	1.84	0.39	1008	2208	1.38	0.22	9670
277.5	257.0	2.35	2357	2.65	0.64	1102	2302	1.14	0.12	7370
388.5	268.4	3.14	0217	3.98	0.81	1220	0020	1.38	0.10	
499.5	275.0	2.74	0356	3.42	0.78	1148	2348	1.38	0.13	
610.5	279.6	2.46	0437	2.80	0.65	1157	2357	1.78	0.26	
721.5	282.0	2.28	0516	2.70	0.70	1204	0004	1.54	0.23	
832.5	283.2	2.02	0536	2.30	0.65	1205	0005	1.51	0.28	
n	297									

Notes: Col. 1 - Mean radius (km) from center of the T_{BB} data.
Col. 2 - Mean T_{BB} (K).
Col. 3 - Standard deviation of the diurnal T_{BB} distribution.
Col. 4 - Time (LST) of maximum amplitude of first harmonic.
Col. 5 - Maximum amplitude of the first harmonic.
Col. 6 - Variance explained by first harmonic.
Col. 7 - Time(s) (LST) of maximum amplitude of second harmonic.
Col. 8 - Maximum amplitude of the second harmonic.
Col. 9 - Variance explained by second harmonic.
Col. 10- Cloud top height (m) based upon Caribbean rainy season atmosphere.
n - Total number of observations.

Table 2. Statistics of the Fourier analysis of the diurnal time series of the mean T_{BB} distribution of Atlantic Ocean hurricanes.

1	2	3	4	5	6	7		8	9	10
55.5	214.1	1.42	1308	1.01	0.25	0758	1958	0.92	0.21	12930
166.5	232.0	1.93	0438	1.38	0.26	0746	1946	1.04	0.15	10703
277.5	251.8	2.50	0402	2.94	0.69	0436	1636	0.92	0.07	8113
388.5	265.2	2.08	0426	2.15	0.53	0446	1646	1.23	0.17	
499.5	272.6	1.40	0420	1.40	0.50	0404	1604	0.46	0.05	
610.5	276.8	1.13	0613	1.19	0.59	0525	1725	0.46	0.09	
721.5	279.0	1.01	0540	1.19	0.69	0545	1745	0.30	0.04	
832.5	280.1	0.81	0734	0.79	0.48	0526	1726	0.33	0.08	
n	239									

Notes: Same as Table 2 legend.

the related statistics appear in Table 1. The first harmonic, on a 24 hour cycle, portrays a diurnal pattern, whereas the second harmonic, on a 12 hour cycle, shows a semidiurnal event. The first and second harmonics explain most of the cloud variance (0.61 to 0.93, Cols. 6 and 9, Table 1).

At the inner core (55.5 km) the first harmonic shows that a diurnal cloud maximum occurs between 0700-0800 LST and a minimum at 1900-2000 LST. Progressing outward from the center this harmonic shows a lag in the diurnal cloud maximum (minimum) at each succeeding radius to 499.5 km where the diurnal cloud maximum (minimum) occurs at 1600 LST (0400 LST). The second harmonic, although quite strong at 166.5 km, becomes increasingly significant in the outer radii (610.5 to 832.5 km) with the semidiurnal cloud maxima (minima) occurring at 0600 and 1800 LST (0000 and 1200 LST). The outward progression of the second harmonic from the center is similar to that of the first harmonic but more rapid. These results show two separate cloud systems exist:

1) a dynamic cloud pattern associated with the inner convection of the tropical storm.
2) a static cloud pattern in the storms environment seemingly unrelated to the inner convection.

The physics of these diurnal and semidiurnal events can be explained by a radiational forcing mechanism (Gray and Jacobson, 1977) and the pressure wave oscillation theory (Brier and Simpson, 1969). The time of occurrence is particularly critical in the physics of the events and is well fixed by the Fourier analysis. At the inner core (55.5 km) of the tropical storm the cloudiness is largely convective and the diurnal pattern of morning maximum and evening minimum compares favorably

with the oceanic, tropical, deep cumulus convection pattern reported by Gray and Jacobson (1977). This pattern is particularly evident when organized mesoscale events, such as the tropical storm, are present. The combined incidence of the morning convective maximum (0700-0800 LST) near the center and the preceding cloud minimum (0400 LST) in the storms environment is responding correctly in time with the radiational forcing mechanism postulated by Gray and Jacobson (1977). Radiational forcing would act to produce extra nighttime tropospheric subsidence in the outer region, suppressing cloudiness, and increasing low-level convergence in the region adjacent to the storm. The resulting increased vapor convergence toward the storm center generates active convection during the morning. The weakened convergence in the adjacent regions during the afternoon (resulting from lesser subsidence) acts to increase the environmental cloudiness and to reduce the afternoon and evening convection near the storm center.

Although the major oscillation of cloudiness in the outer environment of the storm may result from radiational forcing, a lesser but significant pattern appears to result from actions of the solar-lunar tide. The second harmonic shows that this latter activity is most significant in the outer radii (610.5-832.5 km) and that semidiurnal cloud maxima (minima) occur at 0600 and 1800 LST (0000 and 1200 LST). These times compare favorably with the maxima (0700 and 1900 LST) and minima (0100 and 1300 LST) proposed by Brier and Simpson (1969) in the pressure wave oscillation theory. In this, it is postulated that maximum (minimum) cloudiness occurs in response to convergence (divergence) during the period of maximum pressure rises (falls). The semidiurnal activity becomes increasingly obscured with decreased distance from storm center.

An outward modulation of an atmospheric wave originating at the inner core is suggested by the lag of the cloud maximum (minimum) at the successive radii progressing outward to 499.5 km from the center. The outward modulation appears to be accompanied with spreading cirriform clouds which make up the central dense overcast (CDO). These spreading subsiding clouds eventually dissipate as they move outward and the mean T_{BB} of 257 K at 277.5 km suggests this to be near the edge of the cirrus shield (Adler and Fenn, 1976) and the limit of the horizontal spread. The speed of this modulation is near 51 km h^{-1} and is suggestive of an upper tropospheric motion associated with a transverse solenoidal flow (Riehl, 1954). The diurnal pattern of the modulation seemingly causes the diurnal expansion and contraction of the CDO. The expansion of the cloud shield during the day and its contraction at night was investigated by Browner, et al., 1977 using three temperature thresholds (253, 239, 223 K) and found to maximize (minimize) at 1700 LST (0300 LST). These times do not conform well with the same temperature thresholds in this study set where the maximum (minimum) cloudiness occurs at 1000 LST (2200 LST) (Table 1, time of first harmonic minimum and maximum); but, Browner's results included storms of hurricane intensity and it will be shown that there is a more favorable time conformance with the stronger intensity category. This same oscillation of the CDO was noted by forecasters and other investigators and thought to be associated with a diurnal change in wind intensity. Sheets (1972)[1], investigating the diurnal central surface pressure,

---

[1]Sheets, R., 1972: Stormfury Annual Report, App. G, 121-126, NHRC, Coral Gables, FL, 33146.

found no evidence of intensity change. The greatest amplitude of cloud change occurs in the region immediately adjacent (388.5-610.5 km) to the edge of the CDO. Within this region the diurnal cloud maximum (minimum) occurs at near 1600 LST (0400 LST).

Hurricane diurnal variation. A greater uniformity of activity is associated with the hurricane (Fig. 3) than with the tropical storm; however, certain features are evident:

1) a diurnal cloud maximum (minimum) occurs at 0200 LST (2000 LST) at the inner core.
2) maximum diurnal cloud variation occurs at 277.5 km.
3) the outer radii exhibit very little diurnal cloud variation.
4) the strongest mean T_{BB} gradient (greatest change in cloud top height) occurs between 55.5 and 277.5 km.

The cloud patterns associated with the hurricane can be best described using the curves of the first and second harmonics (Fig. 5) and the statistics of the Fourier analysis given in Table 2. In the deep convection near the storm center (55.5 km) a diurnal cloud maximum (minimum) occurs at 0100 LST (1300 LST) as shown by the first harmonic. The contribution to the total variance from this harmonic is weak (0.25) and other harmonics (second, third, fourth) provide a sizeable contribution (0.21, 0.06, 0.10 respectively). From 166.5 km outward to 499.5 km the diurnal cloud maximum (minimum) occurs at 1600 LST (0400 LST) while beyond this distance there is only a slightly later time of occurrence (maximum at 1800-2000 LST, minimum at 0600-0800 LST). A significant semidiurnal maxima (minima) of clouds is evident at the inner part of the hurricane and occur at 0200 and 1400 LST (0800 and 2000 LST). Beyond this distance the maxima (minima) occur at 1100 and 2300 LST (0500 and 1700 LST) and are mostly quite weak.

Great uniformity of convection exists at the hurricane's inner core. This uniformity suggests that steady continual forcing is taking place. The very compact nature of the hurricane is shown by the great difference between the convection pattern at the inner core and that immediately adjacent (166.5 km) to it. The quasi-steady nature of the diurnal cloud pattern from 166.5 km outward and the time of day of the maximum (minimum) suggest that there is a strong influence at these radii due to radiational forcing. A significant semidiurnal oscillation of cloudiness occurs near the storm center (55.5 and 166.5 km) but is not in harmony with any known atmospheric or radiational cycle. The weak semidiurnal oscillation at the greater radii also cannot be reconciled. The variation of the cloud patterns at all radii is slight. The greatest variation occurs at 277.5 km where the mean T_{BB} (252 K) suggests the near proximity of the edge of the CDO. The diurnal cloud maximum (minimum) at this distance occurs at 1600 LST (0400 LST). This temperature range and time of occurrence (at 166.5 km as well as 277.5 km) corresponds closely with the temperature thresholds and time of occurrence of the diurnal expansion and contraction of the CDO found by Browner, et al., (1977).

Summary of diurnal variation results. Upon comparing the results of the review of the cloud and convection patterns associated with the two intensity categories certain common and contrasting features are apparent. The most evident common features are:

1) the strongest convection occurs near the storm center (55.5 km).
2) a great cloud top height change occurs in the first 333 km from the center (tropical storm, 4.6 km; hurricane, 4.8 km). The implied height change (based upon the mean T_{BB}) could be

partially affected by less dense clouds and less dense cloud cover as distance from the center increases.

3) the CDO extends outward to between 222-333 km.

4) diurnal cloud patterns are dominant in the outer environment (499.5-832.5 km).

The major contrasting features are:

1) the deep convection of the hurricane is more uniformly distributed throughout the day than that of the tropical storm.

2) the hurricane does not exhibit the outward modulating wave at the intermediate radii such as that associated with the tropical storm.

3) the greatest cloud oscillation occurs at a radius associated with the edge of the CDO (277.5 km) in the hurricane and at a radius adjacent to the CDO (388.5 km) in the tropical storm.

4) the cloudiness of the hurricane is more uniformly distributed, at all radii, throughout the day than within the tropical storm.

5) the diurnal expansion and contraction of the CDO of the hurricane does not appear to be related with an outward modulation such as that which seemingly occurs within the tropical storm.

6) the mean T_{BB} associated with the hurricane are colder, at each radii, than those of the tropical storm.

7) the first and second harmonics explain less of the variance of the cloud oscillation within the hurricane than within the tropical storm.

8) the greatest cloud top height change occurs between 166.5-277.5 km radius within the hurricane and between 55.5-166.5 km radius within the tropical storm.

The common features delineated illustrate conditions largely already known to exist within tropical cyclones. The horizontal extent of the CDO is, however, now quantitatively measured and found to lie between 222-333 km from the center. Additionally, the major cloud cycle in the storms outer environment is quantitatively defined. The contrasting features delineated suggest that radiational forcing has a prominent role in the convective cycle during the tropical cyclones developmental stages but is of less significance after the storm has reached hurricane intensity. The great uniformity of the cloud patterns associated with the hurricane suggests that steady continual forcing is present and the impact extends to even the outer environment. The colder mean T_{BB} of the hurricanes outer radii compared to those of the tropical storm suggests that there is increased cloudiness present. It is not understood why the tropical storm exhibits an outward modulating wave and the hurricane does not. However, there is evidence in the cloud patterns associated with several storms (Faye, Fig. 6) that such modulation does occur at hurricane intensity, but the cyclic pattern extends over a greater period than 24 hr. This suggests that the modulation within strong storms is the result of dynamics rather than diurnal change. The radius at which maximum cloud top height change takes place shows that the CDO of the hurricane has greater horizontal extent than that of the tropical storm.

b. Temporal sequence of the T_{BB} measurements of tropical cyclone Faye.

The temporal sequence of the T_{BB} measurements of a single storm shows features to exist which are not evident in the composited data. In particular, a long term convective pattern which precedes storm intensification is present. The T_{BB} sequence associated with tropical cyclone Faye illustrates this convective pattern. Faye was selected because a long, unbroken temporal sequence was obtained throughout her life cycle over water. Faye began as a tropical depression on September 18, 1975 well to the east of the Antilles then intensified while moving westward and passed near to the east and north of Bermuda 9-10 days later. The mean T_{BB} (6 hr running means) temporal distribution of each concentric ring around Faye and the central intensity are shown in Fig. 6.

The most evident features in the sequential mean T_{BB} and maximum wind measurements of tropical cyclone Faye are:

1) a short term diurnal pattern of convection (mean T_{BB}) on September 22-23 near the storm center (55.5 and 166.5 km) changes to a long term pattern on September 24 and continues.
2) an outward modulating wave appears to originate at the inner core and enhances the cloud patterns of the intermediate and outer radii.
3) little change in storm intensity occurs while the storm convection is cycling on a diurnal schedule.
4) wind intensity increases after the initial long term burst of convection on September 24 takes place ($\sim$30 hr lag).
5) wind intensity continues to increase even as the inner convection weakens.

Since the convection during the early life of Faye (September 22-23) is cycling diurnally it is believed that radiational forcing has a prominent role in maintaining the convection (there is, however, concern that the time of day of the convection pattern does not coincide well with that expected by radiational forcing). Following this diurnal activity, a long term burst of convection develops and is subsequently followed by two others nearly 48 hr apart in time. From a review of the synoptic conditions associated with Faye there are strong indications that this storm encountered an upper level divergence field more suitable for convection as it interacted with the Tropical Upper Tropospheric Trough (TUTT) (Sadler, 1976) and the initial convective burst followed. The subsequent convective bursts occurred as Faye interacted with transient waves in the westerlies. As an increased amount of latent heat energy became available from the activity during the initial convective burst, Faye began to intensify. Increased winds are evident beginning nearly 30 hr after the onset of the convective burst. Even as the convection weakened (there was still strong convection present), the winds continued to increase. This continued increase in kinetic energy is assumed to result from the ongoing conversion of latent heat energy already produced from past activity as well as from new latent heat energy available from the existing convection. While the wind is still intensifying, a second convective burst develops releasing even more latent heat energy and Faye strengthens further. The intensification continued until Faye reached the cooler surface waters of the middle latitudes where she entered the

westerlies and recurved. Faye remained at maximum wind intensity of 90 kt for 18 hr, then weakened. The final convective burst had little effect upon Faye's weakening winds.

The pattern of the inner core convection shows an outward modulation. Upon close inspection of Fig. 6, it is seen that the wave seemingly merges with and enhances the existing diurnal pattern of the intermediate and outer radii. A Fourier analysis of the time series (not shown) indicates that the outward modulation originating at the inner core slows, weakens, and merges with (or becomes absorbed into) the diurnal pattern at 499.5 km. Beyond this distance, the wave is not distinguishable. Additionally, the analysis shows that there is an increase in the amplitude of the diurnal pattern at the intermediate radii as the trough of the modulating wave approaches the trough of the diurnal cycle. The diurnal cycle at the outer radii of the storm show a cloud maximum (minimum) at 1800 LST (0600 LST).

c. *Latent heat energy and the convective burst.*

Latent heat energy plays a vital role in the development and maintenance of tropical cyclones. Latent heat of condensation is released when the warm moist tropical air ascends in major cumulus towers of tropical cyclones. This heat energy is the primary fuel for tropical cyclones (Dunn and Miller, 1960). Over a period of time the heat energy is converted to potential energy and ultimately a small fraction is converted to kinetic energy. Knowledge of the amount of latent heat release is, therefore, of prime importance for intensity predictions. A qualitative estimate of latent heat release can be made by examining the storm's convection as shown in the satellite imagery. Quantitative measurements of latent heat release are not available, but indices can be obtained from a measure of the vertical motion within the

storm or from the storm's cloud top temperature. The former provides information on the strength of the vertical flow and, therefore, the potential of the convection, and can be calculated from wind and thermal fields of the storm and the surrounding environment. The latter provides a measure of the intensity of the convection and can be obtained from satellite measurements.

In a theoretical numerical model Rosenthal (1978) demonstrated the relationship between low level vertical motion changes and central sea level pressure changes (Fig. 7). The vertical motion (convection) increases precede the pressure falls (intensification). The maximum storm intensity is reached 36 hr after the vertical motion reaches a peak.

Similar results are obtained empirically using the T_{BB} and wind intensity measurements of Atlantic Ocean hurricanes (Fig. 8). The maximum wind intensity and the mean T_{BB} of the major convective area (within 222 km radius) were each composited to show their distribution relative to the time of the storms greatest wind intensity. The convection (mean T_{BB}) and wind intensity profiles show that major convective surges precede wind intensification. Convective maxima (minimum T_{BB}) occur 27 and 60 hr prior to the time maximum storm strength is attained. In each instance, the convective peak precedes a peak in the rate of intensification by 27 hr. A cycle of 33 hr is shown by the peaks which occur during the successive convective bursts. The convective burst (CVB) is broadly defined as a period of prolonged convection near the inner core of a tropical cyclone. The prominence of the CVB within each storm is apparent from a review of the sequential measurements of mean T_{BB} (within 222 km radius) and wind intensity

of nine tropical cyclones of the study set (Fig. 9a-9i)(eight tropical cyclones which either made a landfall or came under extratropical influence within 24 hours after the CVB began are not shown). The mean T_{BB} and maximum winds are plotted as a function of time. The CVB is shown as an enhanced portion of the mean T_{BB} curve. In several instances, at the beginning of the mean T_{BB} record, no measurements were available to show the magnitude of the mean T_{BB} at an earlier time. Since the mean T_{BB} was <230 K, a CVB was assumed to exist. The CVB is rigidly defined as follows:

1) the CVB is identified using the mean T_{BB} within 222 km of storm center.
2) the CVB is a long term event whose duration is $\geq$15 hr. Oscillations of the mean T_{BB} of $\leq$12 hr duration frequently occur and are temporary events.
3) a CVB exists when the mean T_{BB} has declined to and remains at or below 235 K for $\geq$15 hr.
4) temporary oscillations may occur even while the CVB exists but the CVB is regarded to be continuing as long as the mean T_{BB} remains $\leq$230 K.
5) the CVB will eventually reach a peak and weaken. The mean T_{BB}, during the weakening process, will show a warming trend.
6) the CVB has ended when the mean T_{BB} having reached its peak (coldest T_{BB}) now increases to $\leq$230 K, or the mean T_{BB} no longer decreases for a period of 15 hr.

The mean T_{BB} and wind intensity profiles (Fig. 9a-9i) show that multiple CVB's occur in many cases. Following the initial CVB the tropical cyclone intensifies from the depression, or weak tropical storm stage, to strong tropical storm, or even hurricane, stage. Further

acceleration follows the onset of subsequent CVB's. The most prominant features are:

1) storm intensification is most often preceded by a CVB.
2) the lag time between increased convection and increased wind varies from storm to storm.
3) the relationship in the magnitude of the mean T_{BB} vs magnitude of wind intensity varies from storm to storm.
4) temporary oscillations in convection briefly obscure the larger dominant CVB pattern.
5) multiple CVB's occur and each is generally followed by a further increase in wind intensity.
6) the longer the CVB persists, the longer the increased winds continue.

It seems reasonable that during periods of convective bursts as defined by changes in the mean T_{BB} the vertical motion has a net increase and an abundance of latent heat is released. In a simplification of the process, it may be stated that as this added energy is converted to potential, then kinetic energy, the tropical cyclone gains intensity. The magnitude of the intensification is considered to be related to the amount of latent heat energy available. The mean T_{BB} provides an index of this latent heat energy. The empirical results suggest that only the mean T_{BB} measured during periods of increasing convection are highly correlated with future maximum winds. Therefore, using only the data indicated by the enhanced points (dots) on the T_{BB} curves in Figs. 9a-9i and comparing these mean T_{BB} with future maximum winds a quantitative relationship was determined and is given in

Table 3. The magnitude of the intensity categories was stratified by strong (V $\geq$50 kt) and weak storms (V $\leq$50 kt) separately.

Table 3. Relationship (correlation coefficient) of mean T_{BB} vs future wind intensity.

CATEGORY	r	n	t	s
Strong storms (V $\geq$50 kt)	-0.624	56	25.2	6.6
Weak storms (V $\leq$50 kt)	-0.736	27	15.4	5.1

Notes: 1) r is correlation coefficient.
2) n is number of observations.
3) t is the mean lag time (hr).
4) s is the standard deviation in time (hr).

The time lag for best fit of mean T_{BB} and maximum wind varies from storm to storm. This lag is near 25 hr (15 hr) for strong (weak) storms with a standard deviation of near 7 hr (5 hr). The results clearly show that a significant relationship exists between the mean T_{BB} of the convective area of the tropical cyclone and its future intensity. *Since this strong relationship exists only with the mean T_{BB} measured during the period of increasing convection during a CVB* it is particularly important that frequent measurements of the tropical cyclone be available and that the CVB be clearly identified.

d. Summary of diagnostic results.

The mean T_{BB} measurements have permitted an extensive analysis of the tropical cyclone and its environment on a vastly improved spatial and temporal scale available only with geosynchronous satellite observations. The results from this investigation vividly demonstrate that the internal convective activity of the tropical cyclone has a strong impact on the environmental atmosphere at great distances from the storm center. A semidiurnal oscillation of cloudiness is found to

exist in the less disturbed atmosphere well beyond the storms immediate circulation. In the perturbed atmosphere nearer to the storm center only a diurnal pattern of cloudiness is evident. As the storm matures even the cloud patterns very distant from the storm circulation respond to the cycle of activity emanating from the storm center. Radiational forcing is dominant in the early stages of storm development and produces a pattern of maximum early morning and minimum early evening convection at the inner core. Eventually, strong prolonged bursts of convection develop and storm intensification follows.

The significance of the CVB as a precursor of storm intensification is well demonstrated and better establishes the role of the mean T_{BB} measurements as indices of latent heat release. The use of the T_{BB} data as a prognostic parameter is primarily confined to the CVB. Since the cycle of the CVB is nearly 33 hr, its probable recurrence could be projected to provide a qualitative outlook for further storm intensification. The T_{BB} of the tropical cyclone must be monitored frequently in order to recognize the significant convective patterns which lead to storm intensification.

The relationship of the mean T_{BB} with the future maximum wind is statistically significant and a lag of near 25 hr exists between event changes for strong storms and 15 hr for weak storms. The statistical significance of the mean T_{BB}/maximum wind relationships is sufficiently strong to warrant the use of the mean T_{BB} as a predictive parameter.

The mean T_{BB}/maximum wind relationship shown is considered to be a valid representation which exists for tropical cyclones in a tropical atmosphere over warm surface waters. The relationship should not be extended to tropical cyclones under extratropical influence (tropospheric westerlies, warm low tropopause, cool surface waters).

4. PREDICTION RESULTS

The statistical relationship and the associated logic presented in Section 3 illustrates the usefulness of the mean T_{BB} as a predictive parameter for the future wind intensity of a tropical cyclone. This relationship was expanded to develop two predictive techniques-regression and pattern. The techniques were tested with dependent and independent data and the predicted results were compared with results obtained using two persistence prediction techniques. These latter techniques are widely employed for tropical cyclone intensity predictions. Persistence (NC) assumes that there will be no change in the future maximum wind of the tropical cyclone from that which is presently observed; persistence of change (PC) assumes that the change in the future maximum wind for the next forecast period will equal the change which occurred during the past equivalent period.

a. Tropical cyclone wind intensity prediction - regression technique.

The regression technique is based upon predictive equations which were developed from the linear and polynomial relationships between the mean T_{BB} and the future maximum wind data pairs used in Section 3. The general forms of these equations are:

$$V_n = a + bT \qquad (4\text{-}1)$$

$$V_n = a + bT + cV \qquad (4\text{-}2)$$

$$V_n = a + bT + cT^2 \qquad (4\text{-}3)$$

where V_n is the predicted maximum wind n hr after the mean T_{BB} is observed. n = 25 hr (15 hr) for strong (weak) tropical cyclones with a standard deviation of 7 hr (5 hr). Strong (weak) storms have winds of $\geq$50 kt ($<$50 kt) at time of T_{BB} observation.

V is the observed present maximum wind intensity of the tropical cyclone.

T is the observed present mean T_{BB} within 222 km of the tropical cylone center.

a,b,c are the coefficients developed through regression.

The coefficients of regression for the strong and weak storm predictive equations and the statistics of the regression analysis are shown in Table 4.

Several tests have been made to determine the significance of the results; these include F and t statistics, autocorrelation, risk, size, and confidence tests. The F and t statistical values indicate that the significance level is at <1%. Autocorrelation was found to be non-significant in the predictor (T_{BB}). Autocorrelation is

Table 4. Coefficients of the predictive regression equations and statistics of the regression analysis (dependent data).

Equation	Category	a	b	c	r	R	S	n
4-1	Strong	318.30	-1.044		.624	.389	11.1	56
4-2	Strong	237.44	-0.792	.356	.681	.464	10.5	56
4-3	Strong	1913.22	-15.70	.0336	.650	.423	10.9	56
4-1	Weak	270.76	-1.017		.736	.542	6.7	27
4-2	Weak	209.92	-0.798	.364	.777	.604	6.4	27
4-3	Weak	16.99	1.260	-.0051	.737	.543	6.9	27

Notes: 1) a,b,c are the coefficients of regression.
2) r is the correlation coefficient.
3) R is the variance.
4) S is the standard error of the estimate.
5) n is the number of observations.

considered to be important when the correlation coefficient of a sequential data set at lag 1 is >.95. The size and risk test results suggest that the sample set is sufficiently large so that with a 5% risk a tolerable error not exceeding 6 kt can be expected. The confidence interval test suggests that predictive results within 3.5 kt of the standard error can be expected with 99% confidence.

b. Tropical cyclone wind intensity prediction - pattern technique.

The appearance of the CVB was shown to precede maximum wind increases. Following 21 of 22 CVB's of the study set, the maximum wind increased by ≥10 kt within 24 hr. There was little change in the future maximum wind when the CVB was not present. While this technique does not provide the specific magnitude of the wind increase, it does illustrate the significance of the CVB as a precursor to future maximum wind increases.

The contingency table (Table 5) summarizes the frequency of maximum wind change following periods during which the CVB is present (Table 8, which will be discussed later, shows the frequency of future maximum wind change when the CVB was not present). The frequencies shown in Table 5 were determined by finding the magnitude of future maximum wind change 12, 18, 24, 30, and 36 hr after the time of the mean T_{BB} observation of the tropical cyclones of the study set. These results show that a significant maximum wind increase (≥10 kt) occurred 53% of the time within 12 hr and 91% of the time within 36 hr of the mean TBB observation during a CVB in strong storms. Within weak storms the frequency of significant maximum wind increase is 50% at 12 hr and 98% at 36 hr.

Table 5. Pattern technique. Frequency of maximum wind change as a function of time following a CVB for strong (weak) storms (dependent data).

Δt / Δv	12	18	24	30	36
≥10	.47(.50)	.36(.43)	.21(.21)	.16(.25)	.09(.11)
≥10	.53(.50)	.64(.57)	.79(.79)	.84(.75)	.91(.98)
≥20	.11(.11)	.38(.39)	.53(.46)	.56(.57)	.63(.68)
≥30	0(0)	.09(.07)	.28(.25)	.38(.36)	.43(.47)
≥40	0(0)	0(0)	.07(.04)	.20(.15)	.28(.22)
n	53(28)	53(28)	53(28)	50(28)	46(28)

Notes: 1) Δt is expressed in hr.
2) Δv is maximum wind change expressed in kt.
3) weak storms results are enclosed in parentheses.
4) frequency is expressed in present.

c. *Comparison of results.*

The regression equations produced predicted maximum winds with a standard error near 11 kt (7 kt) (Table 4) using the mean T_{BB} as a predictor for strong (weak) storms. The addition of persistence (present maximum wind, Eq. 4-2) as a predictor slightly improved the outcome. In Table 6, the results obtained from the regression equations are compared with the results obtained from persistence (NC) and persistence of change (PC) prediction techniques using the same dependent data set. The results of the regression equation predictions in all cases yielded a lesser error than either of the persistence techniques.

Table 6. Comparison of the mean absolute error and the standard error of the estimate of the regression and persistence techniques (dependent data).

Category	Eq. 4-1	Eq. 4-2	Eq. 4-3	NC	PC
Strong $\overline{\lvert e \rvert}$	9.2	8.8	8.8	17.6*	14.6
σe	11.1	10.5	10.9	12.7	18.4
Weak $\overline{\lvert e \rvert}$	4.8	4.9	4.8	12.2*	9.0*
σe	6.7	6.4	6.9	7.9	9.6

Notes: 1) all values are expressed in kt.
2) *indicates values are biased $\geq$8 kt too low.

The pattern technique was used to predict a wind intensity increase of $\geq$10 kt (the specific magnitude is not known). The contingency table (Table 5) shows that there was an increase in the wind intensity following a CVB 50-91% of the time. The frequency of wind intensification increased with time. This table also shows that results ($<$10 kt change) which would have been obtained from a persistence (NC) technique forecast. The persistence prediction would have yielded a correct forecast $\leq$50% of the time. A contingency table (Table 7) was prepared to show the results obtained with the persistence of change (PC) technique. These results show that the PC technique prediction of $\geq$10 kt wind intensity increase yielded fewer correct results than those obtained with the pattern technique. The pattern technique yielded particularly better results than the climatology technique during the weak storm stage.

Table 7. Persistence of change (PC) technique. Frequency of correct wind intensity forecasts by magnitude as a function of time following a CVB for strong (weak) storms (dependent data).

Δv \ Δt	12	18	24	30	36
≤10	.37(.37)	.23(.22)	.08(.11)	.02(.11)	0(.04)
≥10	.48(.22)	.54(.22)	.56(.22)	.59(.26)	.71(.33)
≥20	.02(0)	.21(0)	.40(0)	.47(0)	.38(0)
≥30	0(0)	.04(0)	.10(0)	.14(0)	.16(0)
>40	0(0)	0(0)	0(0)	.04(0)	.04(0)

Note: See Table 5 notes.

An additional test was made to determine the magnitude of change in wind intensity whenever the CVB was not present. A contingency table of the distribution is shown as Table 8. These results show that there was no change (<10 kt) in wind intensity 64-79% of the time during the next 12-36 hr whenever a CVB was not present. The majority of the wind intensity increases of ≥10 kt occurred with measurements immediately prior to the time the CVB began and the brief periods between CVB's (this suggests that the rigid criteria for defining the CVB may be relaxed to include mean T_{BB} values of >235K as a part of the CVB).

Table 8. Frequency of wind intensity change by magnitude as a function of time when the CVB is not present (all intensity categories considered).

Δv \ Δt	12	18	24	30	36
*(≥10)	.03	.03	.05	.10	.10
<10	.78	.79	.75	.68	.64
≥10	.19	.18	.20	.22	.26
n	78	77	75	73	69

Notes: 1) See Table 5 notes.
2) * indicates decrease in wind intensity.

A skill score (Panofsky and Brier, 1965) for each condition (CVB present or not present) can be determined using:

$$S = \frac{R-E}{T-E} \qquad (4-4)$$

where S is the skill score.

R is the number of correct forecasts.

E is the number of expected correct forecasts based on some standard.

T is the total number of forecasts.

Assuming a standard of 50% of the total forecasts within each category will be correct the skill scores for a forecast increase in wind intensity of $\geq$10 kt were determined for each CVB condition and are compared in Table 9. The negative results associated with the CVB not present condition indicate a forecast of a wind increase when the CVB is not present is likely to be incorrect. The presence of the CVB does, however, improve the likelihood of a successful forecast for a wind increase *and the likelihood of success increases with time* outward to 36 hr. These results further demonstrate that knowledge of the convective pattern as measured by the mean T_{BB} will contribute immensely to the success of an increase/no increase forecast.

Table 9. Comparison of skill score for a wind increase of $\geq$10 kt with the CVB present vs CVB not present as a function of time following the forecast.

Condition \ Δt	12	18	24	30	36
CVB present	.03	.20	.58	.59	.81
CVB not present	-.61	-.66	-.54	-.58	-.50

Note: Δt is expressed in hr.

d. Independent data test results.

An independent data set was compiled to be used as a test of the regression and pattern techniques and for comparison of the results with results obtained using the persistence prediction techniques. The

independent data set is comprised of 96 satellite (mean T_{BB}) observations of six Atlantic Ocean tropical cyclones which occurred during 1976-1979. The mean T_{BB} (within 222 km radius) and the maximum wind profiles are shown as a function of time in Figs. 10a-10f.

The CVB(s) is delineated according to the convention ascribed in Section 3 as an enhanced part of the mean T_{BB} profile. The specific mean T_{BB} values used for prediction are further enhanced as a dot on the temperature profile. The predicted wind intensity obtained using the regression and persistence techniques for strong and weak storms for each individual forecast are shown in Tables 10 and 11, respectively, in the interest of comparison of specific cases. The mean absolute forecast errors are summarized in Table 12. These results show that the regression technique yielded lesser errors in the wind intensity prediction for strong and weak storms at all time periods except one (the PC forecast for weak storms at 12 hr yielded a lesser error than regression). The lesser error of the regression forecasts is as much as 13 kt to as little as 3.9 kt for strong storms and as much as 10.6 kt to as little as 3.4 kt for weak storms (one time period, PC at 12 hr, excepted).

The mean absolute error of the regression forecasts for the strong storms for the 18, 24, and 30 hr periods is 15.3 kt. This value exceeds the mean standard error (10.8 kt) of the dependent test set by 4.5 kt or 1 kt more than the maximum error expected from the confidence interval test. The maximum is exceeded by 2.6 kt for the weak storms. The tolerable error of 6 kt (which assumes a 5% risk) is not exceeded for strong storms but is exceeded by 0.1 kt for weak storms. Since the sample independent data set is small, these results are not sufficiently statistically significant, yet it is encouraging to find that the predictions yield errors near or within the acceptable statistical bounds.

The pattern technique also yielded better results than the persistence techniques. The contingency table developed for the pattern technique shows that wind intensity increases of $\geq$10 kt occurred 58-71% of the time following a CVB (Table 13). The persistence (NC) technique ($<$10 kt change) would have produced correct predictions only 8-33% of the time. The contingency table for the persistence of change forecast (Table 14) shows that the PC technique would have yielded a correct prediction of wind intensity of $\geq$10 kt 46-50% of the time; or 12-21% less often than the pattern technique.

Table 10. Predicted wind intensity using regression and persistence techniques (independent data). Strong storms only.

1	2	3	4	5	6	7	8	9	10	11	12	13
Frederic	1500	9/11	91	94	87	90	107	112	117	113	115	115
Frederic	2100	9/11	99	106	98	98	118	123	128	115	115	105
Ella	1200	8/31	77	76	80	60	80	90	100	100	110	110
Ella	1800	8/31	80	82	80	70	90	100	110	110	110	105
Ella	1200	9/1	86	100	83	110	150	160	165	100	80	70
Ella	1300	9/1	88	102	88	110	150	160	165	100	80	70
Ella	0000	9/3	73	76	79	70	40	35	30	95	110	115
Ella	1200	9/3	80	87	80	85	100	90	70	115	120	115
Ella	1500	9/3	82	94	84	90	110	105	90	118	117	110
Ella	1800	9/3	88	96	85	95	115	115	110	115	105	80
Cora	1200	8/8	78	73	80	50	75	75	80	80	70	65
Cora	1800	8/8	81	81	81	65	105	105	105	70	65	60
Gloria	0900	9/28	72	72	79	60	80	87	92	63	65	68
Gloria	1200	9/28	77	76	80	60	75	85	90	65	65	70
Gloria	1500	9/28	80	78	80	60	70	80	87	65	68	75
Gloria	1800	9/28	80	78	80	60	65	75	85	65	70	80
Gloria	2100	9/28	84	81	82	60	62	70	80	68	75	83
Gloria	1200	9/29	88	86	85	65	65	65	65	85	90	90
Gloria	1500	9/29	88	87	85	68	68	68	68	88	90	90
Gloria	1800	9/29	92	91	89	70	80	80	80	90	90	90
Gloria	2100	9/29	92	92	89	75	87	90	90	90	90	87
Gloria	1500	9/30	97	102	95	90	105	112	115	87	82	77
Gloria	2100	9/30	97	102	95	90	97	105	108	82	77	72
Anita	2100	8/30	98	95	96	68	101	108	113	78	80	83

Notes: Col. 1 - Name of tropical cyclone.
Col. 2 - Time (GCT) of satellite observation.
Col. 3 - Date (GCT) of satellite observation.
Col. 4,5,6 - Predicted wind (kt) using regression Eqs. 4-1, 4-2, 4-3, respectively.
Col. 7 - Predicted wind (kt) using persistence (NC) technique.
Col. 8,9,10 - Predicted wind (kt) 18, 24, and 30 hr later respectively using persistence of change (PC) technique.
Col. 11,12,13 - Observed wind (kt) 18, 24, and 30 hr later respectively.

Table 11. Predicted wind intensity using regression and persistence techniques (independent data). Weak storms only.

1	2	3	4	5	6	7	8	9	10	11	12	13
Cora	0600	8/8	29	29	30	30	35	35	40	65	80	80
Bess	1200	8/6	36	37	36	30	35	40	40	40	40	40
Bess	1800	8/6	47	47	47	35	40	45	50	40	40	45
Gloria	0300	9/27	49	46	49	28	36	36	36	40	50	58
Gloria	0600	9/27	49	47	49	30	40	40	40	45	55	60

Notes: Cols. 1-7 - See legend of Table 10.
Cols. 8,9,10 - Predicted wind (kt) 12, 18, and 24 hr later respectively using persistence of change (PC) technique.
Cols. 11,12,13 - Observed wind (kt) 12, 18, and 24 hr later respectively.

Table 12. Summary of mean absolute forecast error (kt) for strong and weak storms (independent data).

Method \ Δt	18	24	30	12*	18*	24*
Eq. 4-1	15.6	16.3	15.3	12.0	13.8	15.4
Eq. 4-2	13.0	15.6	15.0	10.8	14.6	16.2
Eq. 4-3	15.6	16.3	15.2	11.8	13.6	15.2
NC	16.9	20.5	21.8	15.4	22.4	26.0
PC	17.5	23.8	28.0	8.8	15.8	17.4
n	24	24	24	5	5	5

* indicates weak storms results.
n is number of cases tested.
Δt is expressed in hr.

Table 13. Pattern technique. Frequency of wind intensity change by magnitude as a function of time following a CVB for strong storms (independent data).

Δv \ Δt	18	24	30	36
*(≥10)	.08	.13	.17	.29
<10	.33	.21	.13	.08
≥10	.58	.67	.71	.63
≥20	.46	.46	.46	.42
≥30	.17	.17	.17	.13
>40	.08	.13	.08	.08

Notes: 1) See Table 5 notes.
2) * indicates wind intensity decreased.

Table 14. Persistence of change (PC)technique. Frequency of correct wind intensity forecasts by magnitude as a function of time following a CVB for strong storms (independent data).

Δv \ Δt	18	24	30	36
<10	.13	0	0	0
≥10	.46	.50	.50	.50
≥20	.21	.21	.21	.29
≥30	0	.08	.04	.08
≥40	0	0	.04	.04

Note: 1) See Table 5 notes.

c. *Summary of prediction results.*

The values of the mean T_{BB} of the inner convective area (222 km radius of center) of a tropical cyclone which are measured during the period of a CVB while convective activity is intensifying were used to develop regression equations and a pattern technique for predicting the future wind intensity of the storm. The statistical tests suggest that the regression equations will yield high quality results with significance at $< 1\%$ level with great confidence. Following a convective burst as high as 46% of the variance of the future maximum wind of strong storms and 60% of the variance of weak storms is explained by the mean T_{BB} and the present wind intensity. The mean absolute error obtained with the regression equations is considerably lower than those obtained using persistence prediction techniques. The pattern technique predicts intensification of ≥ 10 kt and yields greater success than the persistence techniques.

The prediction results obtained by regression techniques in this investigation of the Atlantic Ocean tropical cyclones can be compared with the results obtained in the Pacific Ocean (Gentry et al., 1980) using the Nimbus satellite data. The prediction errors for strong storms at the 24 hr forecast period are summarized in Table 15. Since the Pacific Ocean tropical cyclone prediction technique differed from that of the Atlantic Ocean method some difference in the results would be expected. The mean T_{BB} measurements of the Pacific Ocean tropical cyclones were in reality opportunity observations where the convective burst was not considered and could not be recognized with the 12 or 24 hr temporal resolution obtained from the polar orbiting Nimbus

satellites. It is, therefore, most encouraging to find, that even without consideration of the convective burst, the Pacific Ocean results compare favorably with those of the Atlantic Ocean. Both the Atlantic Ocean and Pacific Ocean results using the mean T_{BB} as a predictive parameter yielded lesser forecast error than the persistence techniques.

Table 15. Comparison of prediction error (kt) of the Atlantic Ocean and the Pacific Ocean (Gentry et al., 1980) tropical cyclones obtained using regression equations.

Predictive Parameter(s)	Atlantic	Pacific	P-A	Category
T	11.1	11.4	0.3	dependent
T	16.3	18.8(15.8)	2.5(-0.5)	independent
T ,V	10.5	9.4	-0.9	dependent
T ,V	15.6	16.1(11.8)	0.5(-3.8)	independent

Note: Figures in parenthesis assume removal of a bias in the Pacific Ocean study.

The success of the forecast with the Pacific Ocean data without consideration for the CVB suggests that the variability of the internal activity of tropical cyclones within different ocean basins is not the same. The Pacific Ocean results were obtained by using all of the available mean T_{BB} measurements for prediction. Good quality results in the Atlantic Ocean could be obtained by using only the mean T_{BB} measurements made during a CVB for prediction. The recurrence of the CVB during the life cycle of the Atlantic Ocean tropical cyclones is suggestive of interaction with atmospheric events in the storm's environment. It is probable that the greater forcing associated with the larger and more intense Pacific Ocean typhoons overwhelms other atmospheric events.

5. CONCLUSIONS

The mean T_{BB} of the tropical cyclone and its environment measured from a geosynchronous satellite is highly useful in describing the convection and cloud activity associated with the storm. The high temporal resolution provides a sequential quantitative measure of the storm's changing conditions. It would not be possible to monitor this activity as completely with a polar orbiting satellite.

The cloudiness associated with the tropical cyclone is marked primarily by diurnal activity resulting from diurnal convective changes within the storm and long term bursts of convective activity produced by atmospheric forcing. Although there are significant cloud and convection patterns within and around the tropical cyclone, the feature with the greatest prognostic significance is the convective burst. The relationship of the intensity of the convection (mean T_{BB} of the inner convective area) measured during the convective burst to future storm intensity has been well demonstrated and has strong statistical significance. The physical processes which produce the convection/intensity relationship are sound but because satisfactory quantitative measures of convection have been lacking, a workable prognostic relationship has not previously been developed. The mean T_{BB} is helpful in this respect since it does provide a quantitative measure of the strength of the convection. Additionally, the identification of the useable (for intensity prediction) T_{BB} measurements further enhances its utility for intensity prognosis.

The regression technique yielded wind intensity forecasts with a smaller error than the forecasts made with the persistence techniques. Additionally, the ability to correctly forecast a wind intensity

increase (or no change) with great confidence using the pattern technique is regarded to be of great value. The good quality of these results require consideration for the use of the regression and pattern techniques in operational forecasting.

The modulating wave produced by the inner core convection has been frequently observed in the satellite imagery. It was not known, however, that the modulation continued so far beyond the storms immediate circulation. The effect of the modulating wave (which is not restricted to tropical cyclone activity only) suggests that the cyclic nature of the varying cloud patterns which exist in the atmosphere may depend upon proximity to an organized disturbance. Semidiurnal cloud patterns are likely to exist in the less disturbed atmosphere, a diurnal cloud pattern (afternoon maximum) in a disturbed atmosphere near an organized disturbance, and a diurnal pattern of convection (morning maximum) within an organized disturbance. Even in this, the time of day of a particular occurrence is likely to vary depending upon the distance of the observation point from an organized system.

Acknowledgements. The authors appreciate the dedicated assistance of the computer specialists, particularly Mr. Raymond Morris, for their assistance in compiling the mean T_{BB} results from the more than 1400 computer tapes of satellite data. Typing and modification of the several drafts of this paper by Miss Vicky Chin and Mrs. Cora Lee Sawyer is greatly appreciated. The review of this report by Drs. Joanne Simpson and Robert Adler is appreciated.

REFERENCES

Adler, R. F., and D. D. Fenn, 1979: Thunderstorm intensity as determined from satellite data. J. Appl. Meteor., 18, 502-517.

Adler, R. F., and E. B. Rodgers, 1977: Satellite-observed latent heat release in a tropical cyclone. Mon. Wea. Rev., 105, 956-963.

Black, P. G. and R. A. Anthes, 1971: On the asymmetric structure of the tropical cyclone outflow layer. Mon. Wea. Rev., 99, 1348-1366.

Brier, G. W., and J. Simpson, 1969: Tropical cloudiness and precipitation related to pressure and tidal variations. Quart. J. Roy. Meteor. Soc., 95, 120-147.

Browner, S., W. L. Woodley and C. G. Griffith, 1977: Diurnal oscillation of the area of cloudiness associated with tropical storms. Mon. Wea. Rev., 105, 856-864.

Dunn, G. E., and B. I. Miller, 1960: Atlantic Hurricanes. Louisiana State University Press, 123 pp.

Dvorak, V. R., 1975: Tropical cyclone intensity analysis and forecasting from satellite imagery. Mon. Wea. Rev., 103, 421-427.

Gentry, R. C., E. Rodgers, J. Steranka, and W. Shenk, 1980: Predicting tropical storm intensity using satellite measured equivalent blackbody temperature of cloud tops. Mon. Wea. Rev., 108, 445-455.

Gray, W. M., and R. W. Jacobson, Jr., 1977: Diurnal variation of deep cumulus convection. Mon. Wea. Rev., 105, 1171-1188.

Kidder, S. Q., W. M. Gray, and T. H. Vonder Haar, 1978: Estimating tropical cyclone central pressure and outer winds from satellite microwave data. Mon. Wea. Rev., 106, 1458-1464.

Panofsky, H. A., and G. W. Brier, 1965: Some Applications of Statistics to Meteorology. The Pennsylvania State University, 224 pp.

Riehl, H., 1954: Tropical Meteorology. McGraw-Hill, 392 pp.

Rodgers, E. B., and R. F. Adler, 1981: Tropical cyclone rainfall characteristics as determined from a satellite passive microwave radiometer. Mon. Wea. Rev., 109, 506-521.

_____, R. C. Gentry, W. E. Shenk, and V. Oliver, 1979: The benefits of using short-interval satellite images to derive winds for tropical cyclones. Mon. Wea. Rev., 107, 575-584.

_____, and R. C. Gentry, 1983: Monitoring tropical cyclone intensity using environmental wind fields derived from short-interval satellite images. Mon. Wea. Rev. (to be published in May 1983).

Rosenthal, L., 1978: Numerical simulation of tropical cyclone developent with latent heat release by the resolvable scales. I: Model description and preliminary results. J. Atmos. Sci., 35, 258-271.

Sadler, J. C., 1976: Tropical cyclone initiation by the tropical upper tropospheric trough. Mon. Wea. Rev., 104, 1266-1278.

Short, D. A., and J. M. Wallace, 1980: Satellite-inferred morning-to-evening cloudiness changes. Mon. Wea. Rev., 108, 1160-1169.

Smith, C. L., 1975: On the intensification of hurricane Celia (1970). Mon. Wea. Rev., 103, 131-147.

CAPTIONS

Figure

1 Grid superimposed on a satellite image of hurricane Ella

2 Diurnal mean T_{BB} distribution of Atlantic Ocean tropical storms. Mean radius of the data from storm center is given in the right margin

3 Diurnal mean T_{BB} distribution of Atlantic Ocean hurricanes. Mean radius of the data from hurricane center is given in the right margin

4 First (solid) and second (dotted) harmonics of the diurnal mean T_{BB} distribution of Atlantic Ocean tropical storms. Amplitude (K) of the harmonic is given in left margin. Mean radius of data from storm center is given in the right margin

5 First (solid) and second (dotted) harmonics of the diurnal mean T_{BB} distribution of Atlantic Ocean hurricanes. Amplitude (K) of the harmonic is given in the left margin. Mean radius of data from hurricane center is given in the right margin

6 Temporal sequence of the mean T_{BB} measurements and central intensity (dotted curve) of tropical cyclone Faye. Mean radius (km) of T_{BB} data from storm center is given to right of curve

7 Comparison of vertical motion with central pressure in a model hurricane (Rosenthal, 1978)

8 Composited mean T_{BB} (within 222 km radius) and wind intensity distribution relative to time tropical cyclones first reached maximum intensity (17 cases)

Figure

9 Mean T_{BB} (within 222 km radius) and wind intensity profiles as a function of time. The enhanced portions of the T_{BB} curve show convective bursts. Enhanced T_{BB} points (dots) are used for wind intensity predictions. (a) Hurricane Carmen, 1974. (b) Tropical storm Elaine, 1974 (c) Hurricane Fifi, 1974. (d) Hurricane Eloise, 1975 (e) Hurricane Faye, 1975. (f) Hurricane Gladys, 1975 (g) Hurricane Emmy, 1976. (h) Hurricane Dorothy, 1977 (i) Hurricane Evelyn, 1977

10 Mean T_{BB} (within 222 km radius) and wind intensity profiles as a function of time. The enhanced portions of the T_{BB} curve show convective bursts. Enhanced T_{BB} points (dots) are used for wind intensity predictions. (a) Hurricane Gloria, 1976. (b) Hurricane Anita, 1977 (c) Tropical storm Bess, 1978. (d) Hurricane Cora, 1978 (e) Hurricane Ella, 1978. (f) Hurricane Frederic, 1979

CAPTIONS

Table

1 Statistics of the Fourier analysis of the diurnal time series of the mean T_{BB} distribution of Atlantic Ocean tropical storms

2 Statistics of the Fourier analysis of the diurnal time series of the mean T_{BB} distribution of Atlantic Ocean hurricanes

3 Relationship (correlation coefficient) of mean T_{BB} vs. future wind intensity

4 Coefficient of the predictive regression equations and statistics of the regression analysis (dependent data)

5 Pattern technique. Frequency (expressed in percent) of maximum wind change (Δv) as a function of time following a CVB for strong (weak) storms (dependent data)

6 Comparison of the mean absolute error and standard error of the estimate of the regression, persistence, and climatology techniques (dependent data)

7 Climatology technique. Frequency of correct wind intensity forecasts (expressed in percent) by magnitude as a function of time following a CVB for strong (weak) storms (dependent data)

8 Frequency of wind intensity change (expressed in percent) by magnitude as a function of time when the CVB is not present (all intensity categories considered)

9 Comparison of skill score for a wind increase of $\geq$10 kt with the CVB present vs CVB not present as a function of time following the forecast

10 Predicted wind intensity using regression, persistence, and climatology techniques (independent data). Strong storms only

11 Predicted wind intensity using regression, persistence, and climatology techniques (independent data). Weak storms only

Table

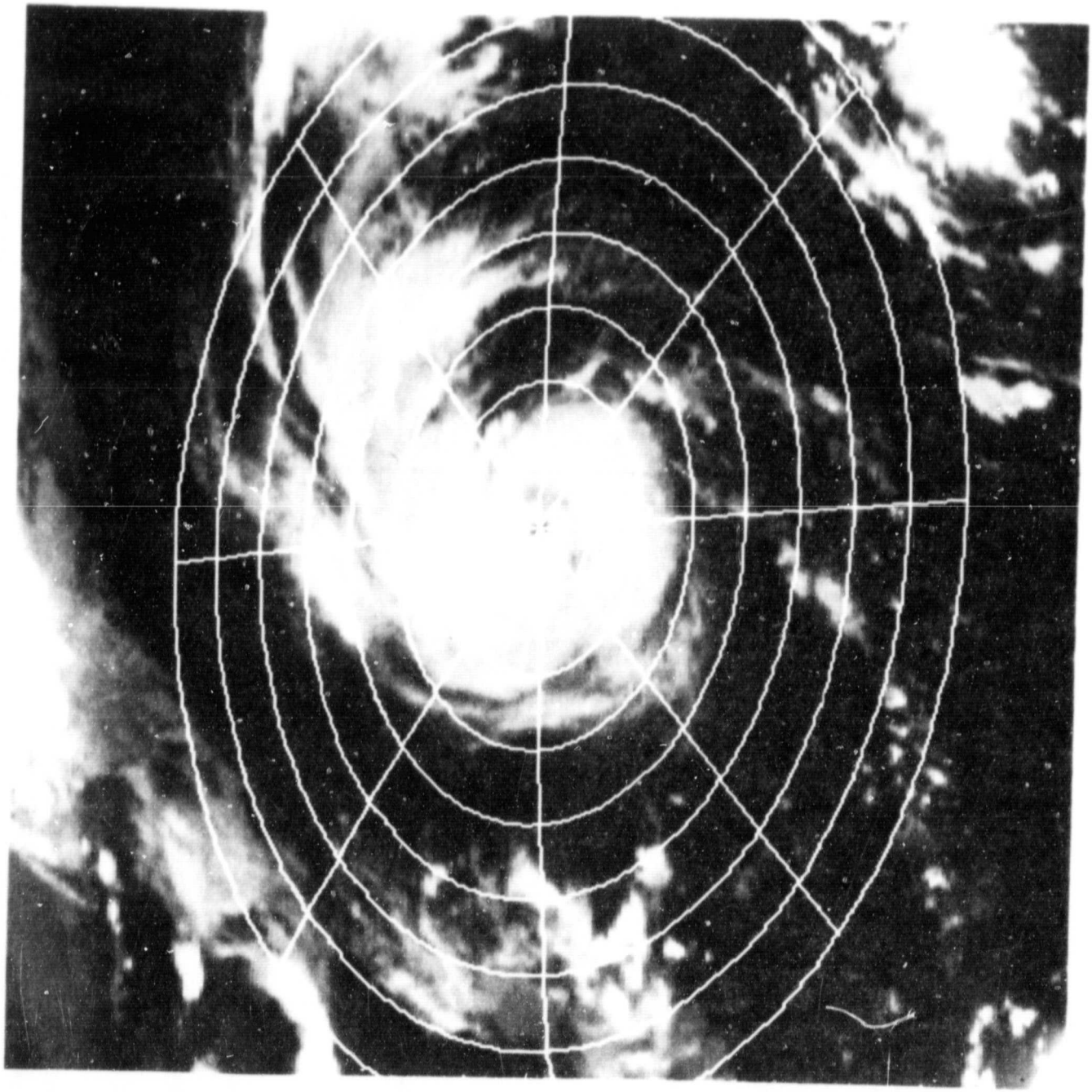

Figure 1. Grid superimposed on a satellite image of hurricane Ella.

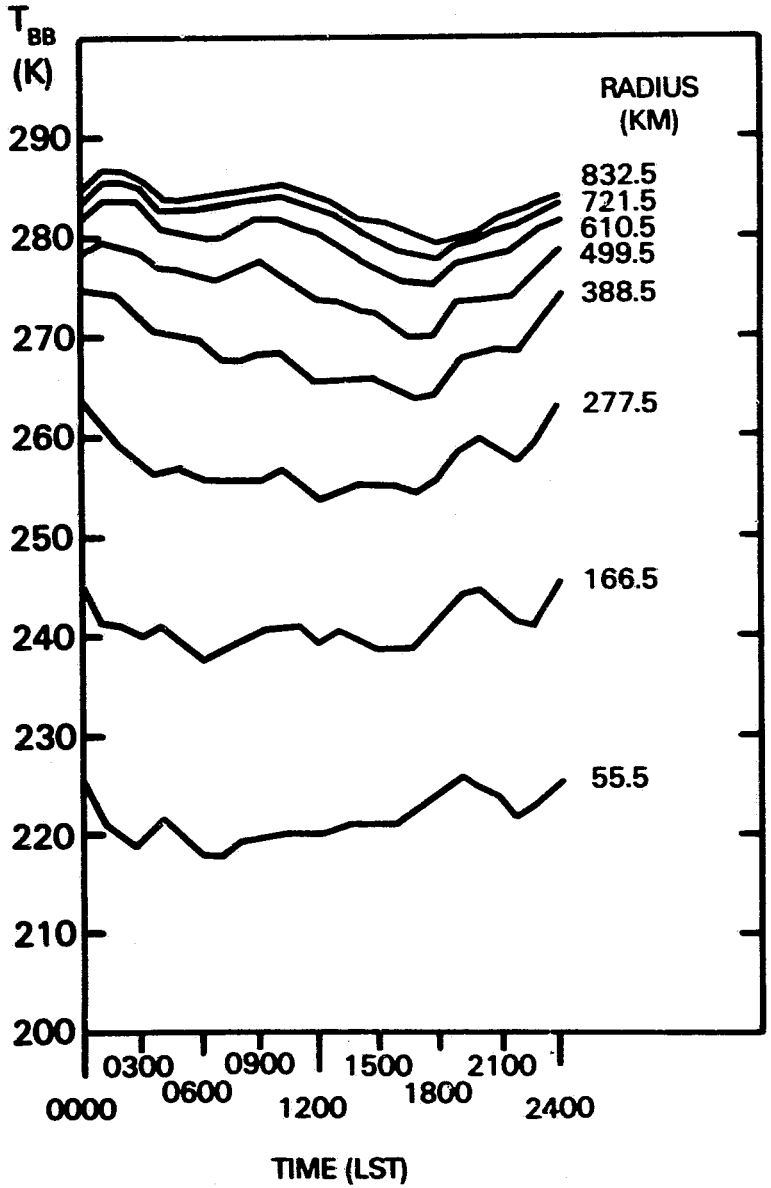

Figure 2. Diurnal mean T_{BB} distribution of Atlantic Ocean tropical storms. Mean radius of the data from storm center is given in the right margin.

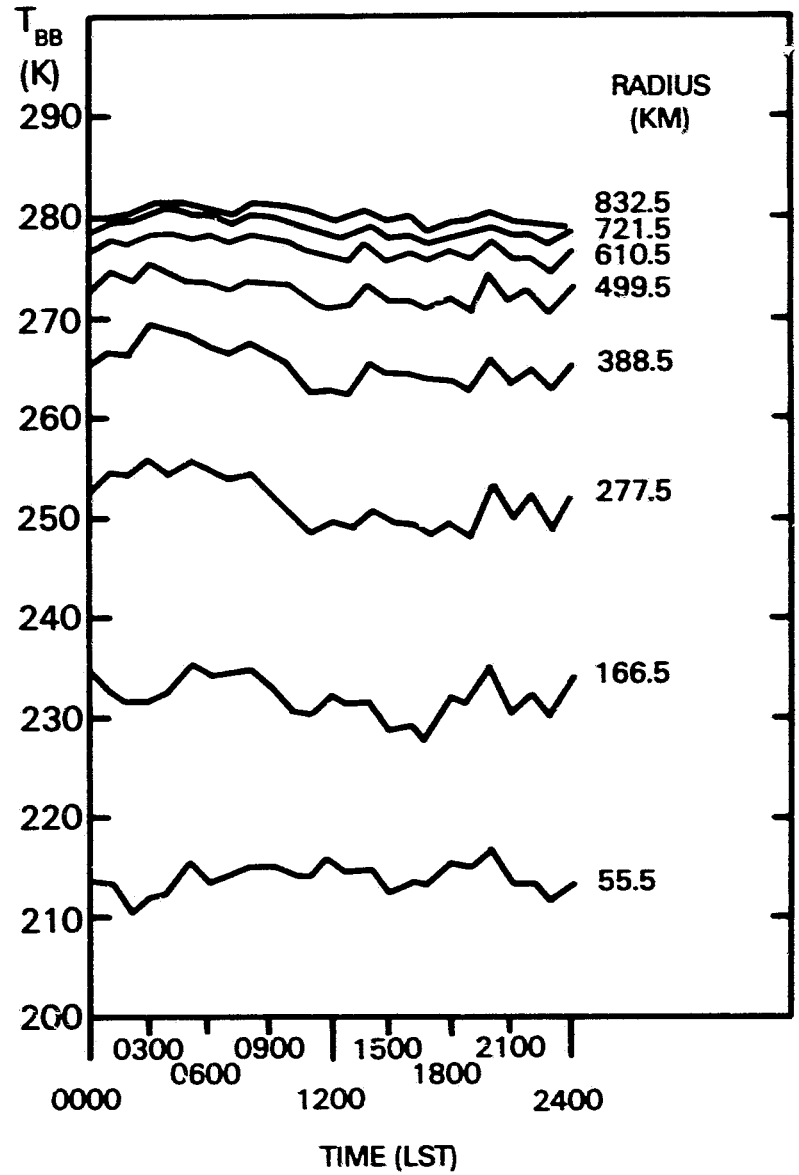

Figure 3. Diurnal mean T_{BB} distribution of Atlantic Ocean hurricanes. Mean radius of the data from hurricane center is given in the right margin.

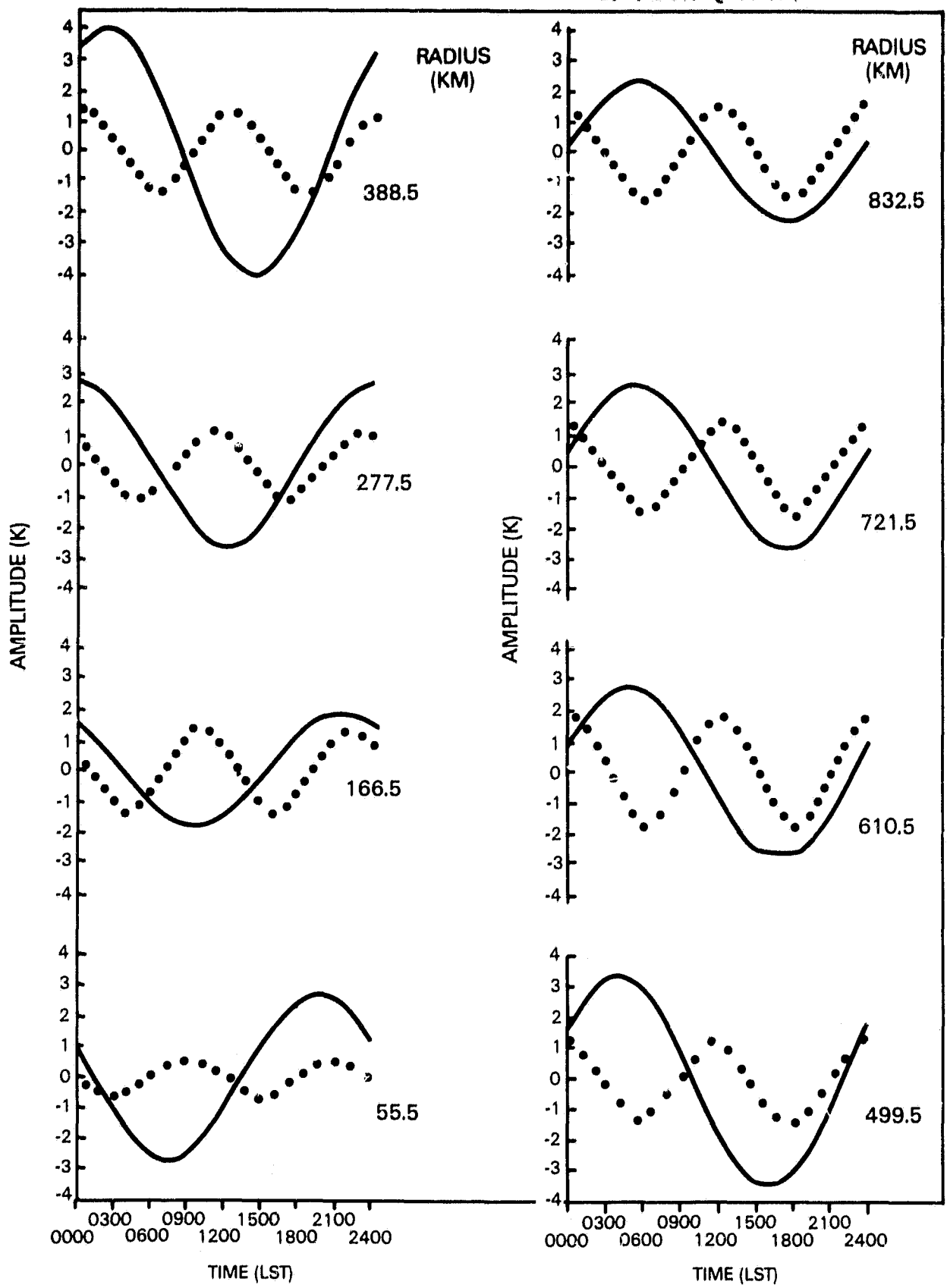

Figure 4. First (solid) and second (dotted) harmonics of the diurnal mean T_{BB} distribution of Atlantic Ocean tropical storms. Amplitude (K) of the harmonic is given in left margin. Mean radius of data from storm center is given in the right margin.

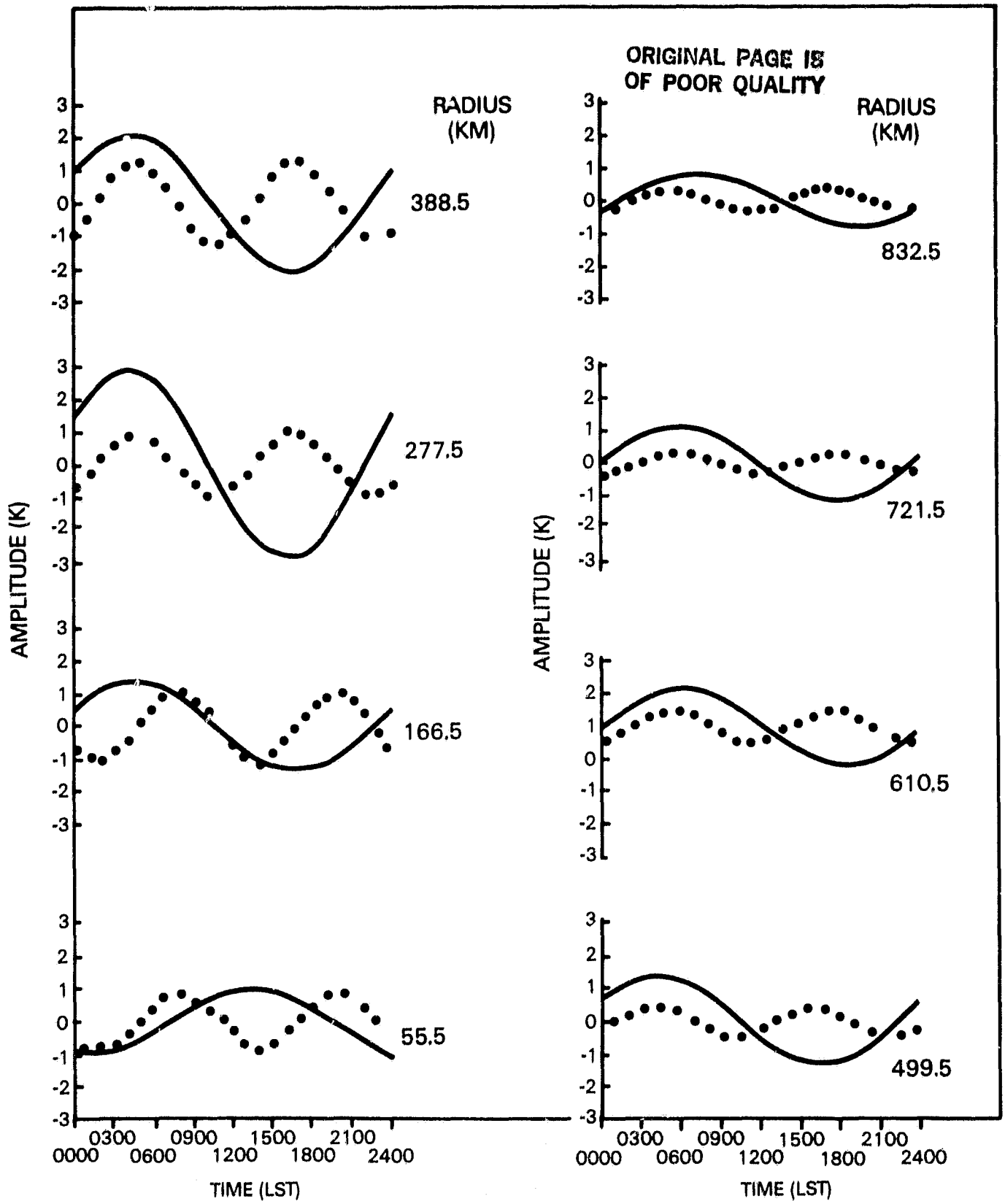

Figure 5. First (solid) and second (dotted) harmonics of the diurnal mean T_{BB} distribution of Atlantic Ocean hurricanes. Amplitude (K) of the harmonic is given in the left margin. Mean radius of data from hurricane center is given in right margin.

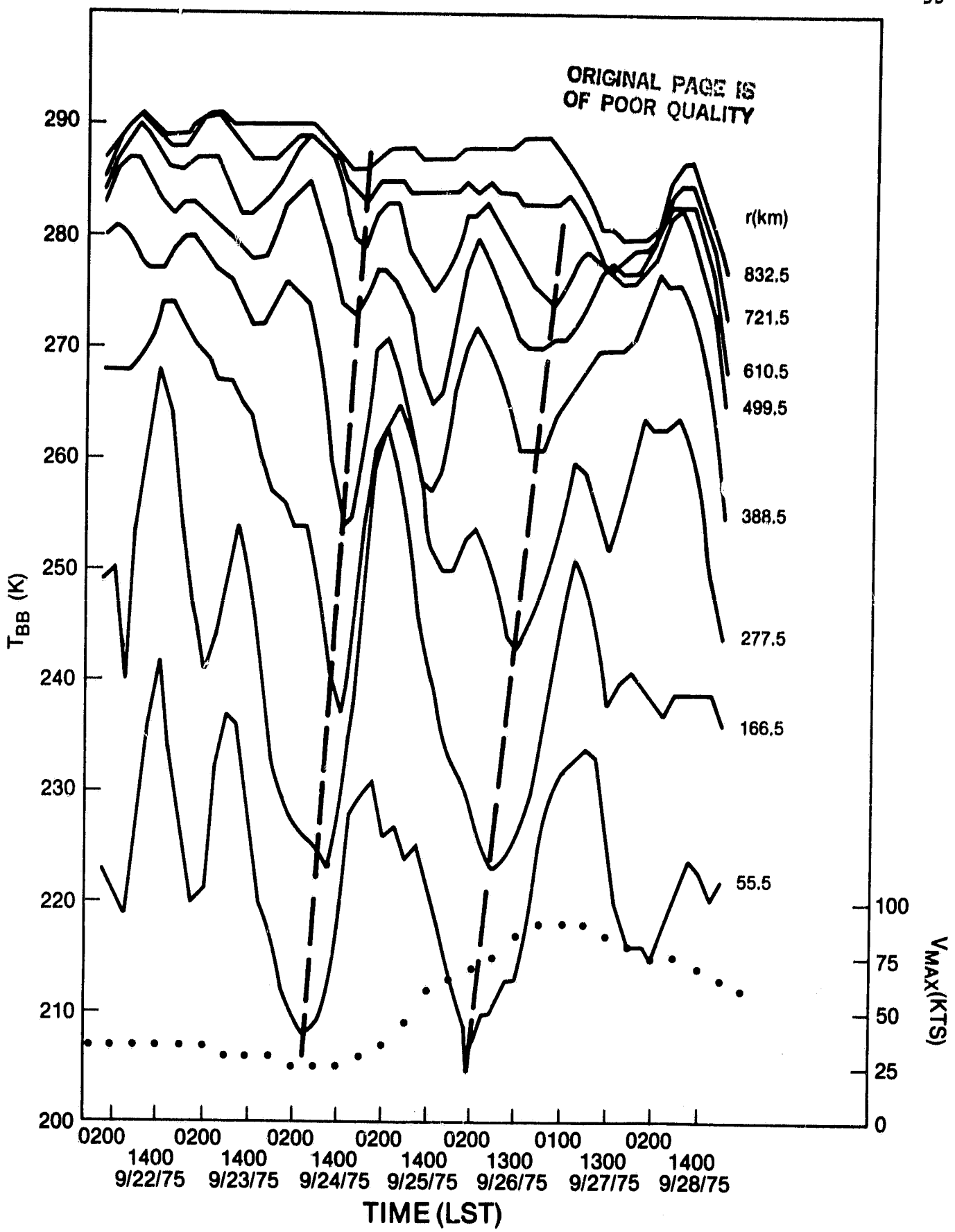

Figure 6. Temporal sequence of the mean T_{BB} measurements and central intensity (dotted curve) of tropical cyclone Faye. Mean radius (km) of T_{BB} data from storm center is given to right of curve.

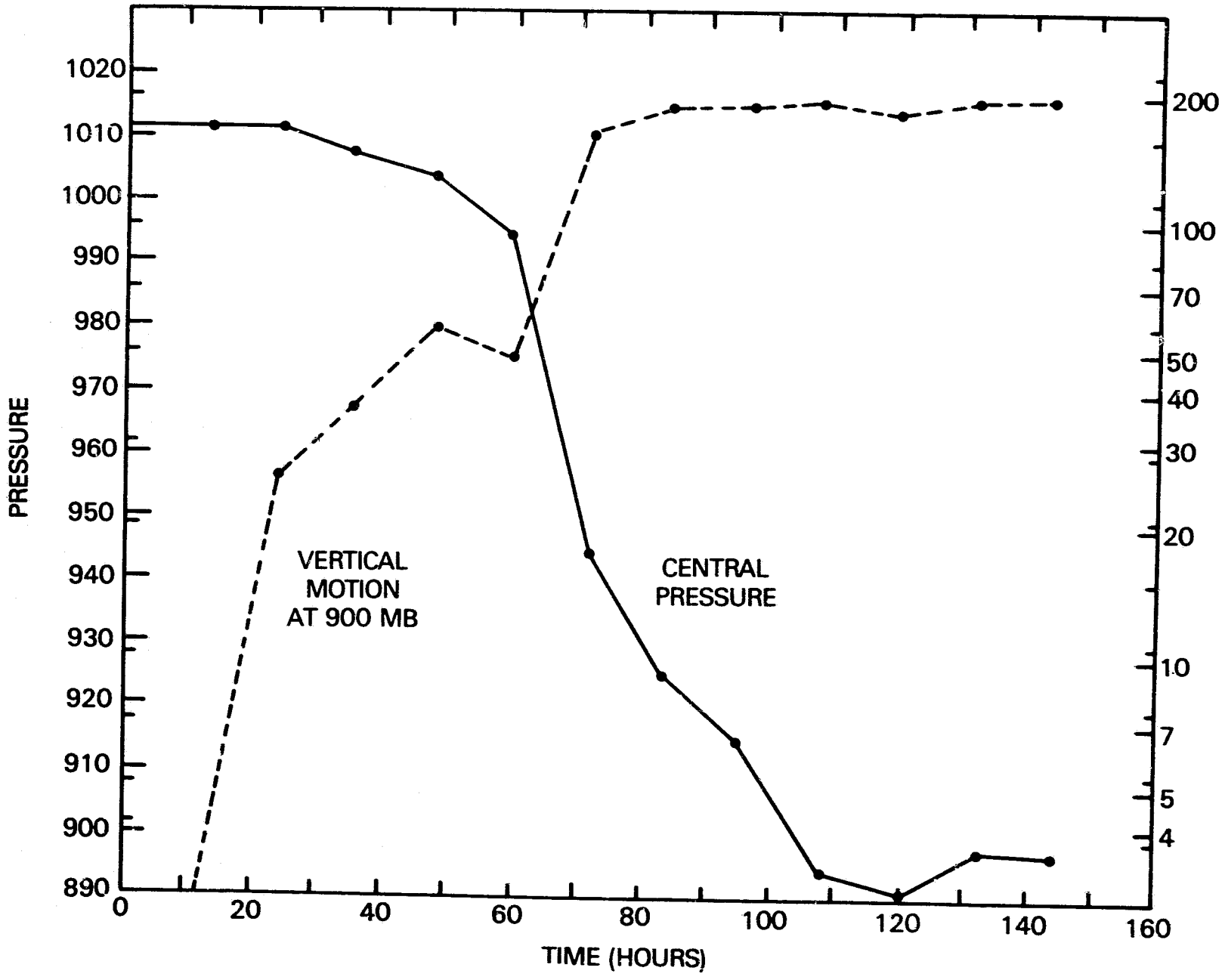

Figure 7. Comparsion of vertical motion with central pressure in a model hurricane (Rosenthal, 1978).

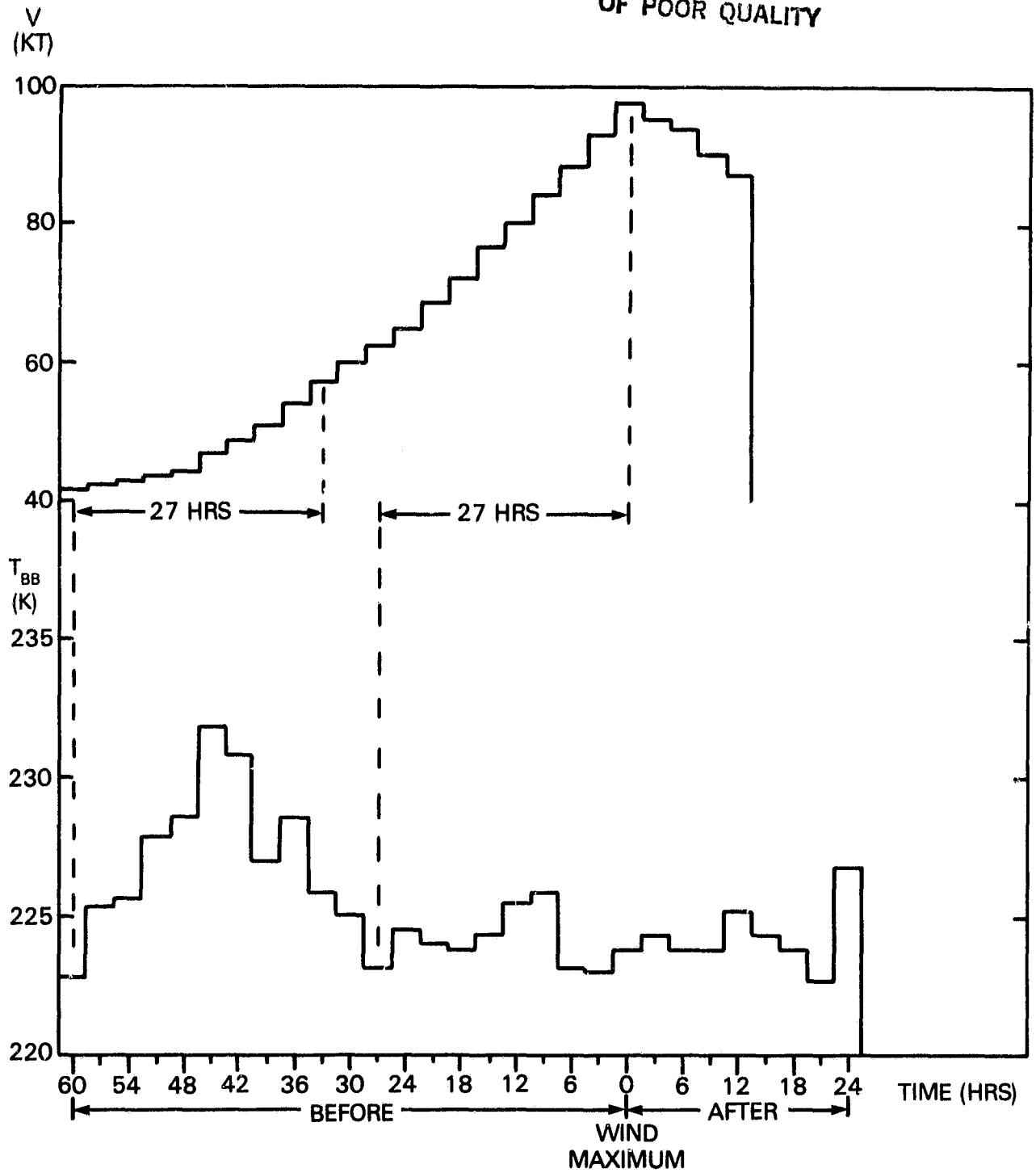

Figure 8. Composited mean T_{BB} (within 222 km radius) and wind intensity distribution relative to time tropical cyclones first reached maximum intensity (17 cases).

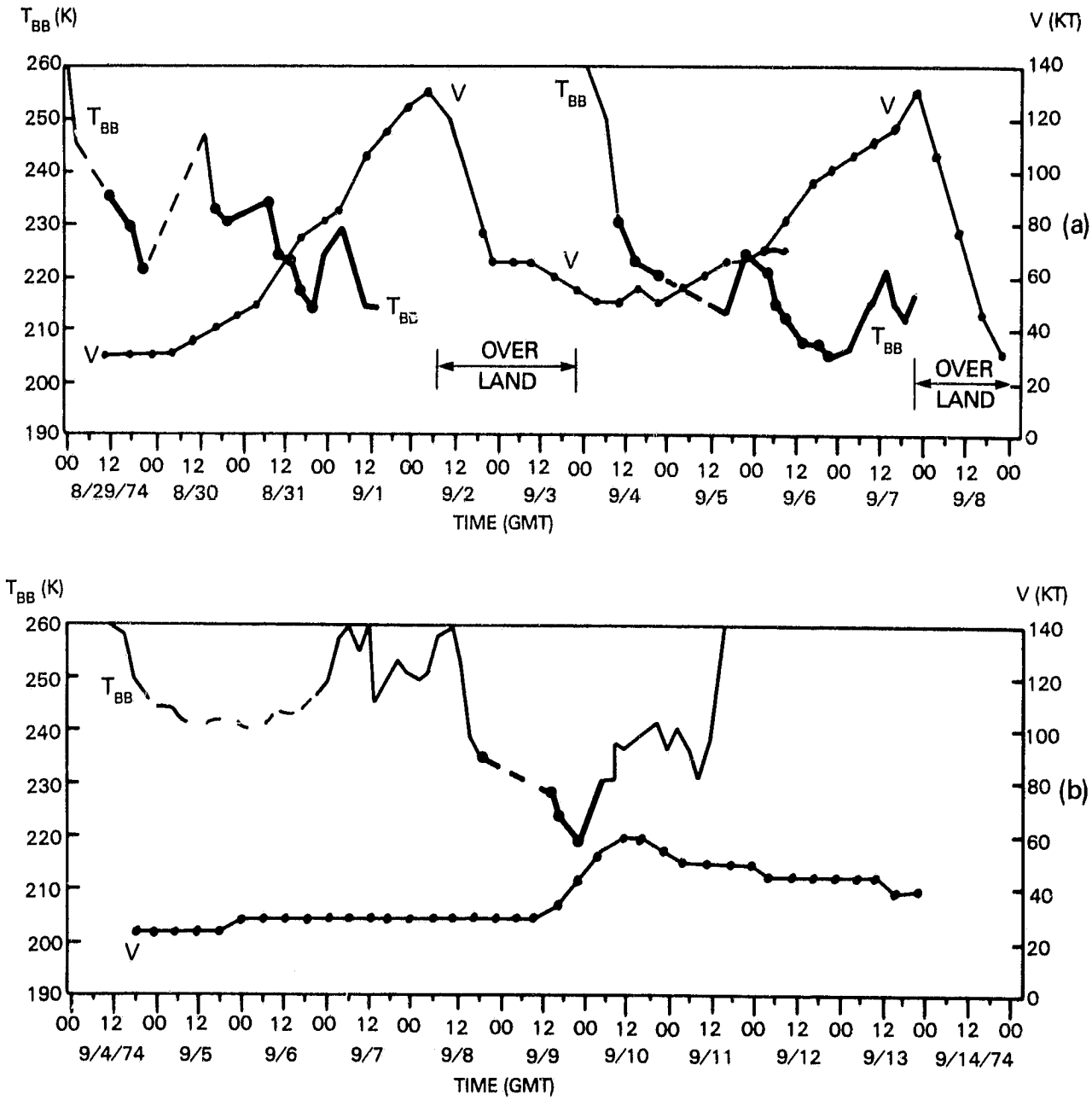

Figure 9. Mean T_{BB} (within 222 km radius) and wind intensity profiles as a function of time. The enhanced portions of the T_{BB} curve show convective bursts. Enhanced T_{BB} points (dots) are used for wind intensity predictions. (a) Hurricane Carmen, 1974. (b) Tropical storm Elaine, 1974.

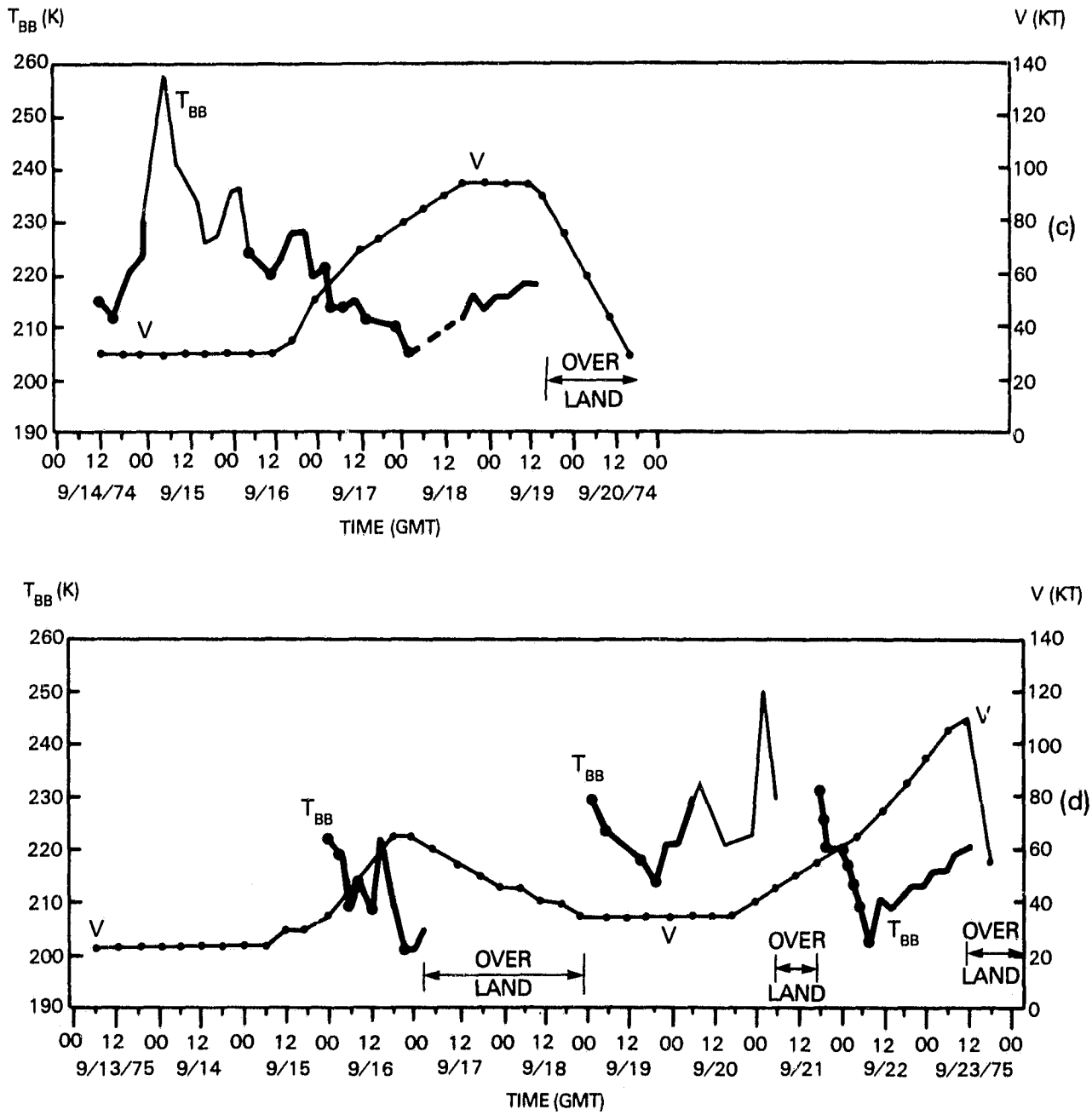

Figure 9. (c) Hurricane Fifi, 1974. (d) Hurricane Eloise, 1975.

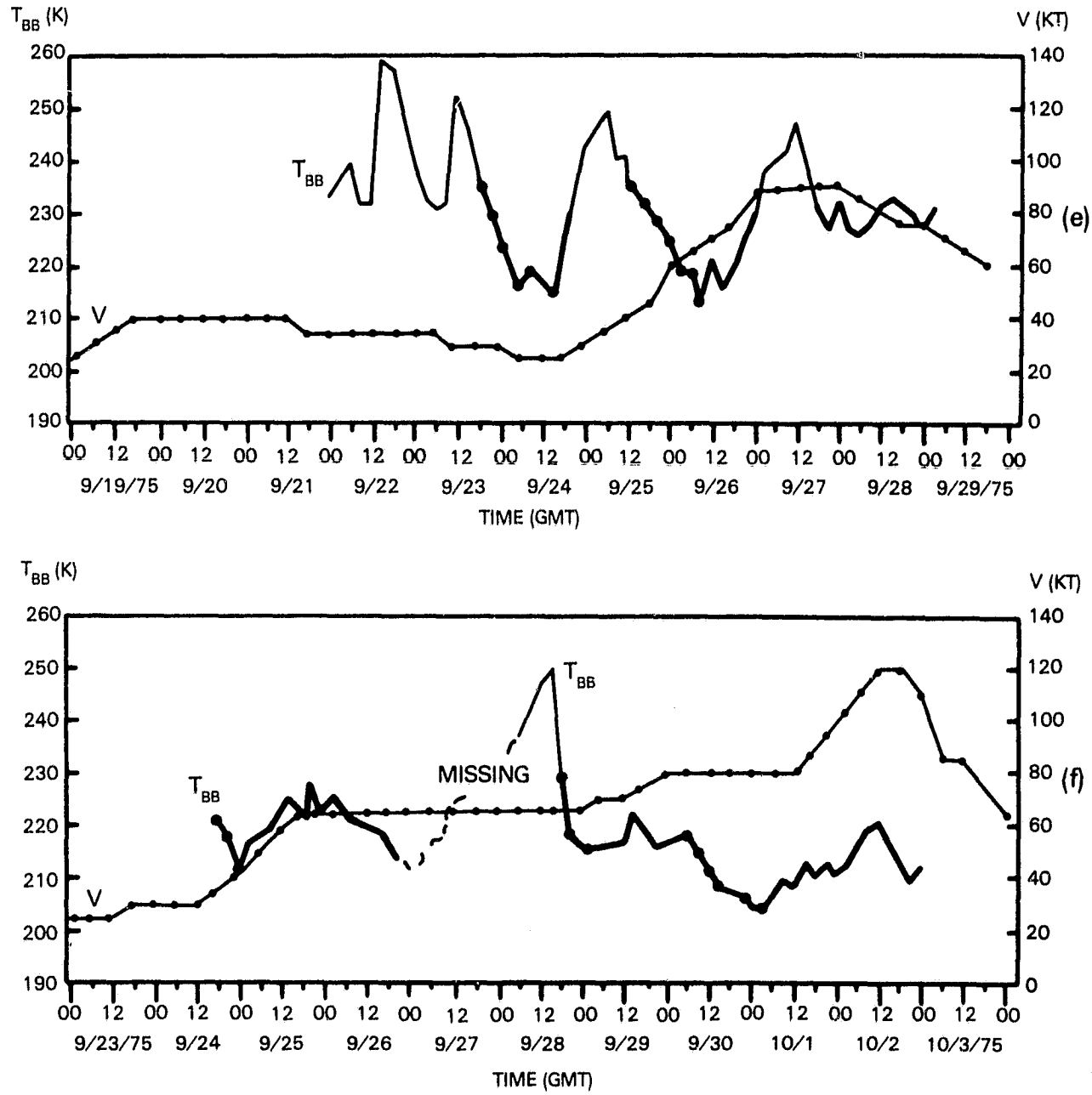

Figure 9. (e) Hurricane Faye, 1975. (f) Hurricane Gladys, 1975.

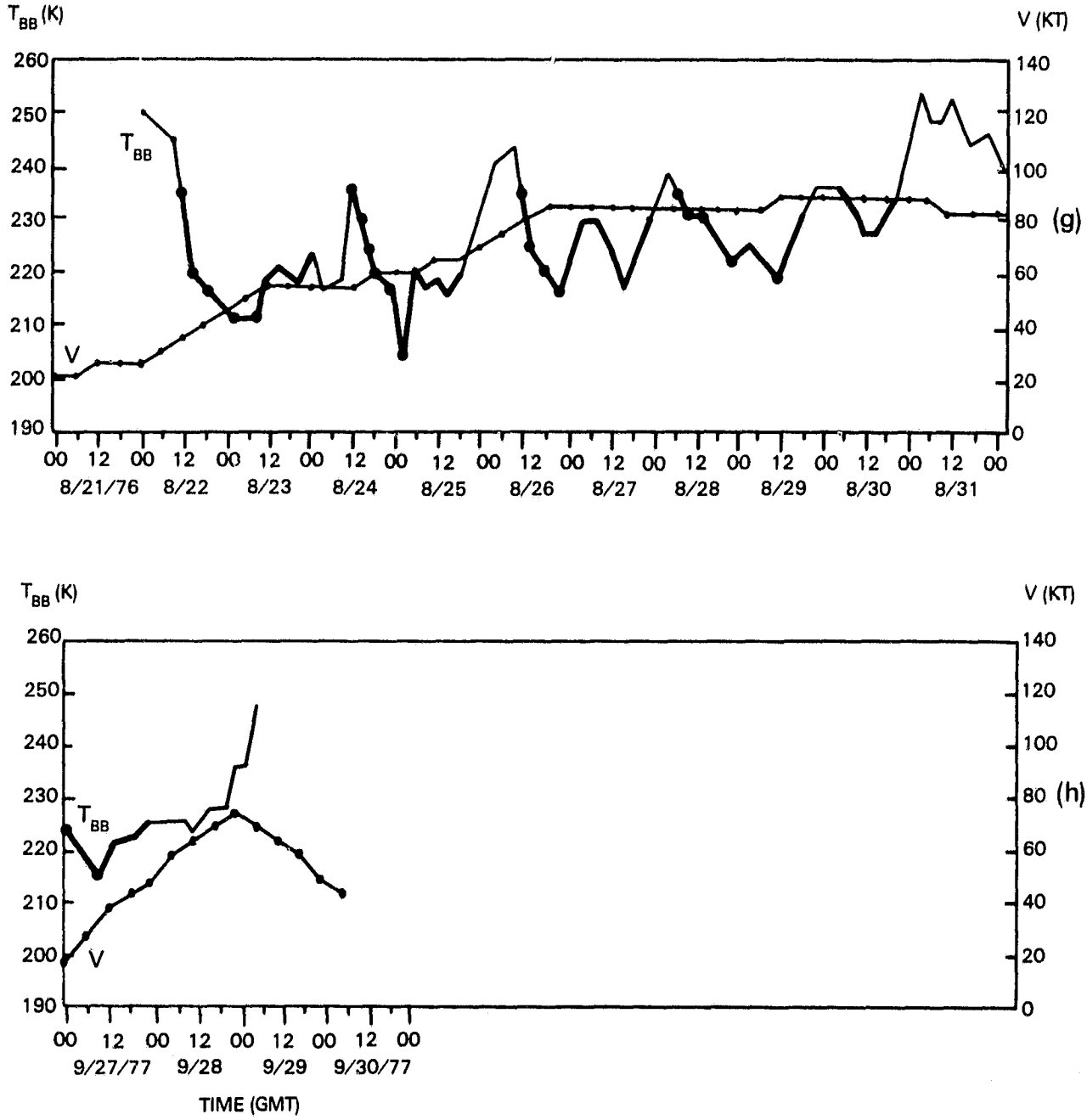

Figure 9. (g) Hurricane Emmy, 1976. (h) Hurricane Dorothy, 1977.

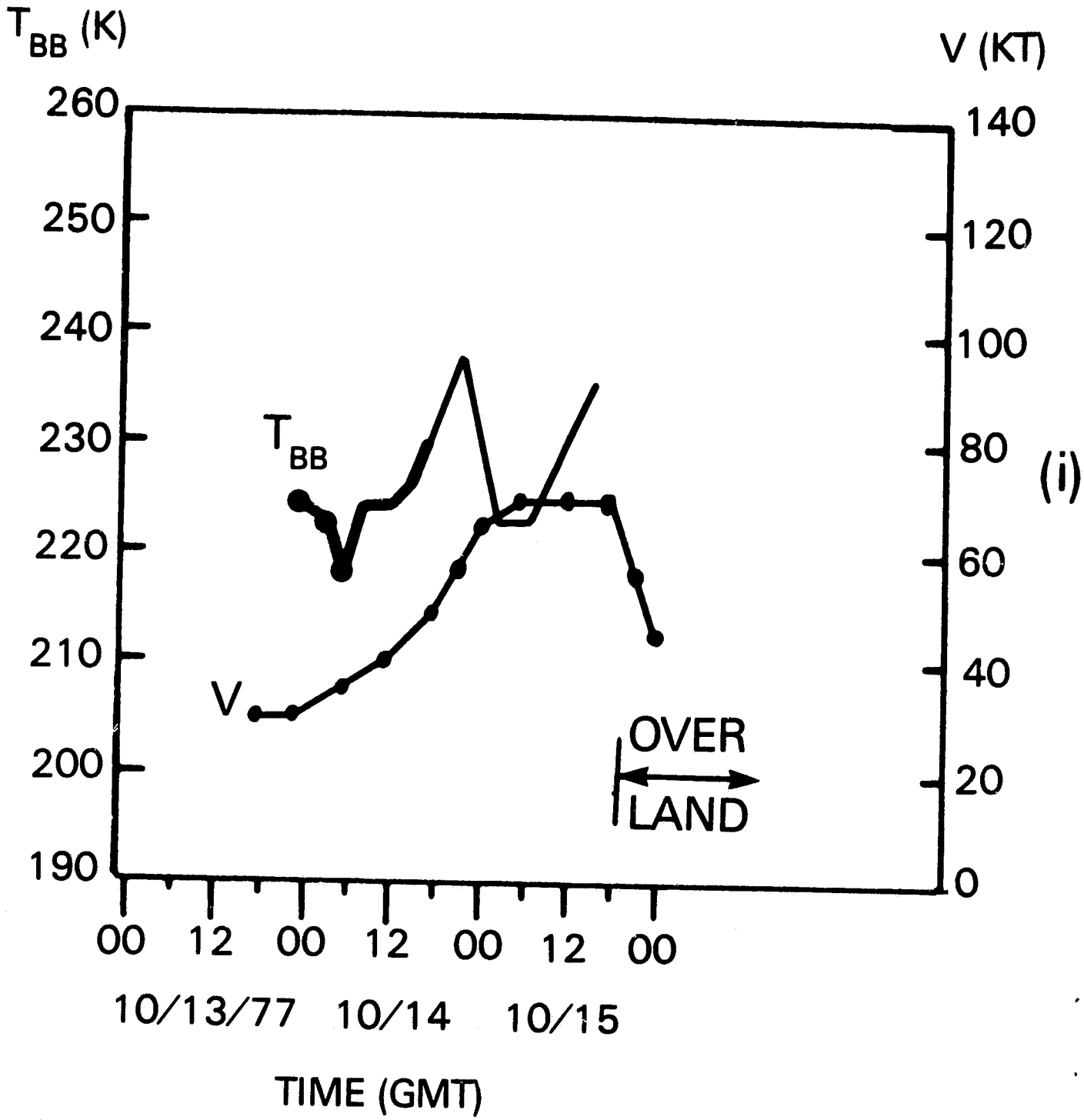

Figure 9. (i) Hurricane Evelyn, 1977.

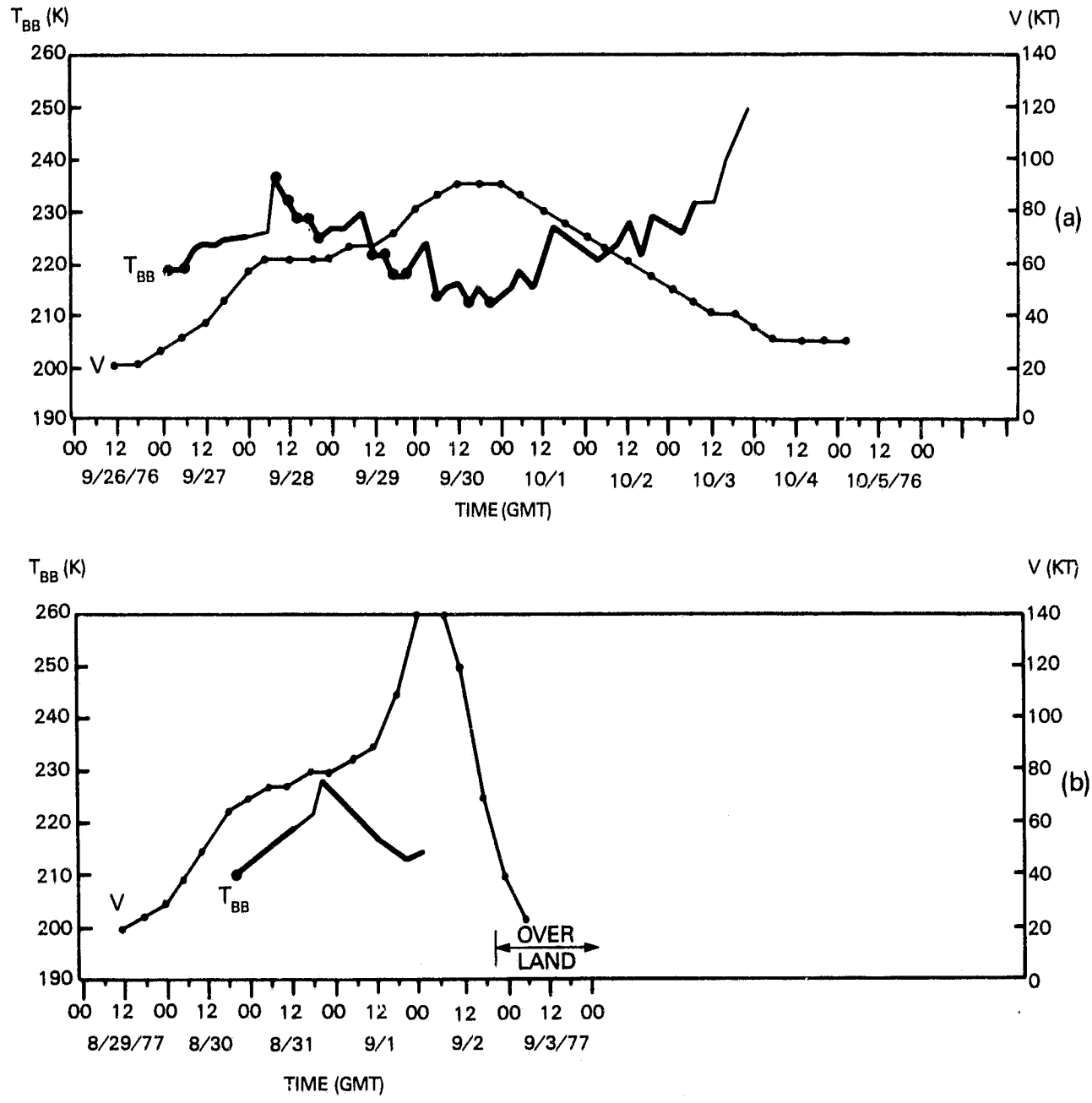

Figure 10. Mean T_{BB} (within 222 km radius) and wind intensity profiles as a function of time. The enhanced portions of the T_{BB} curve show convective bursts. Enhanced T_{BB} points (dots) are used for wind intensity predictions. (a) Hurricane Gloria, 1976. (b) Hurricane Anita, 1977.

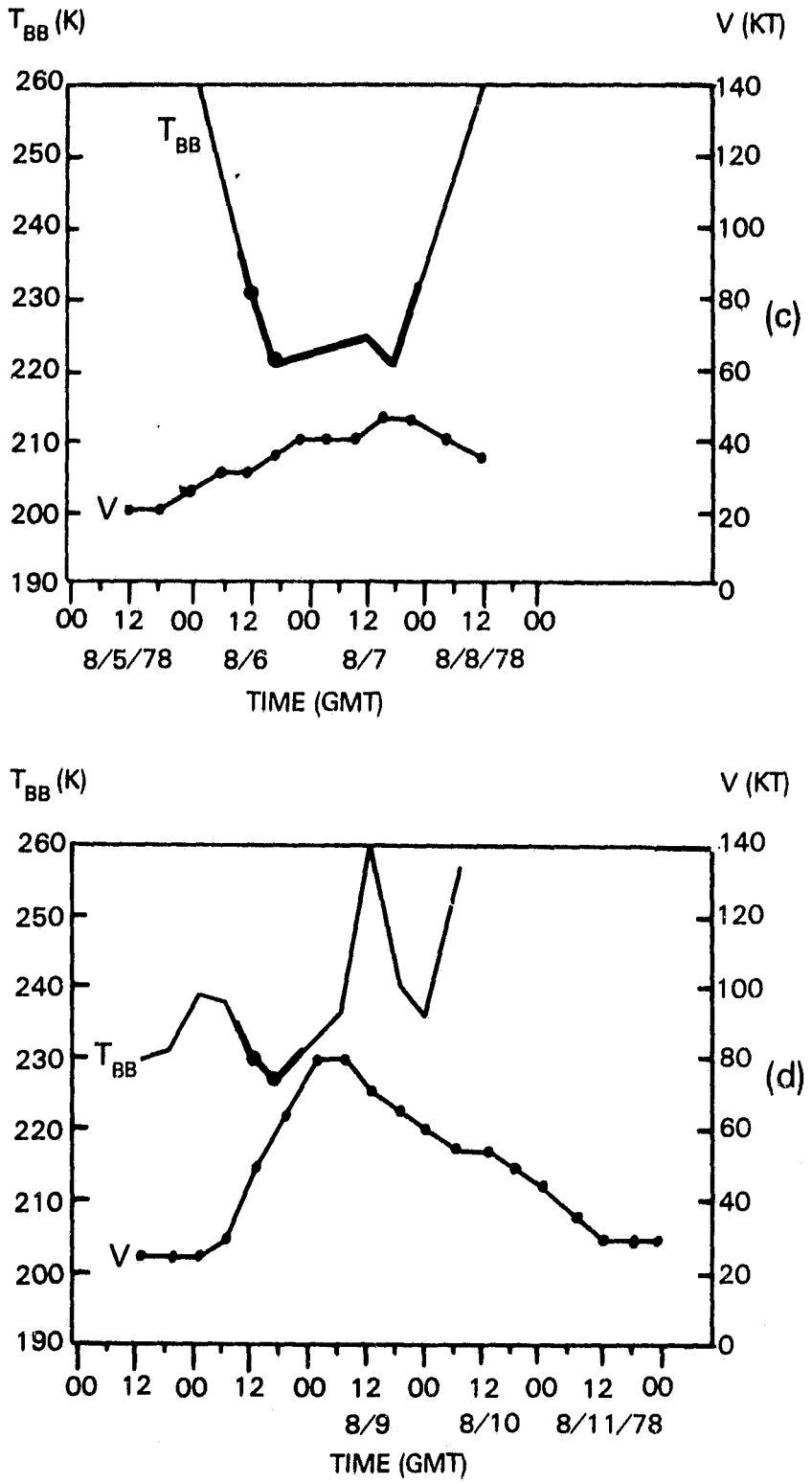

Figure 10. (c) Tropical storm Bess, 1978. (d) Hurricane Cora, 1978.

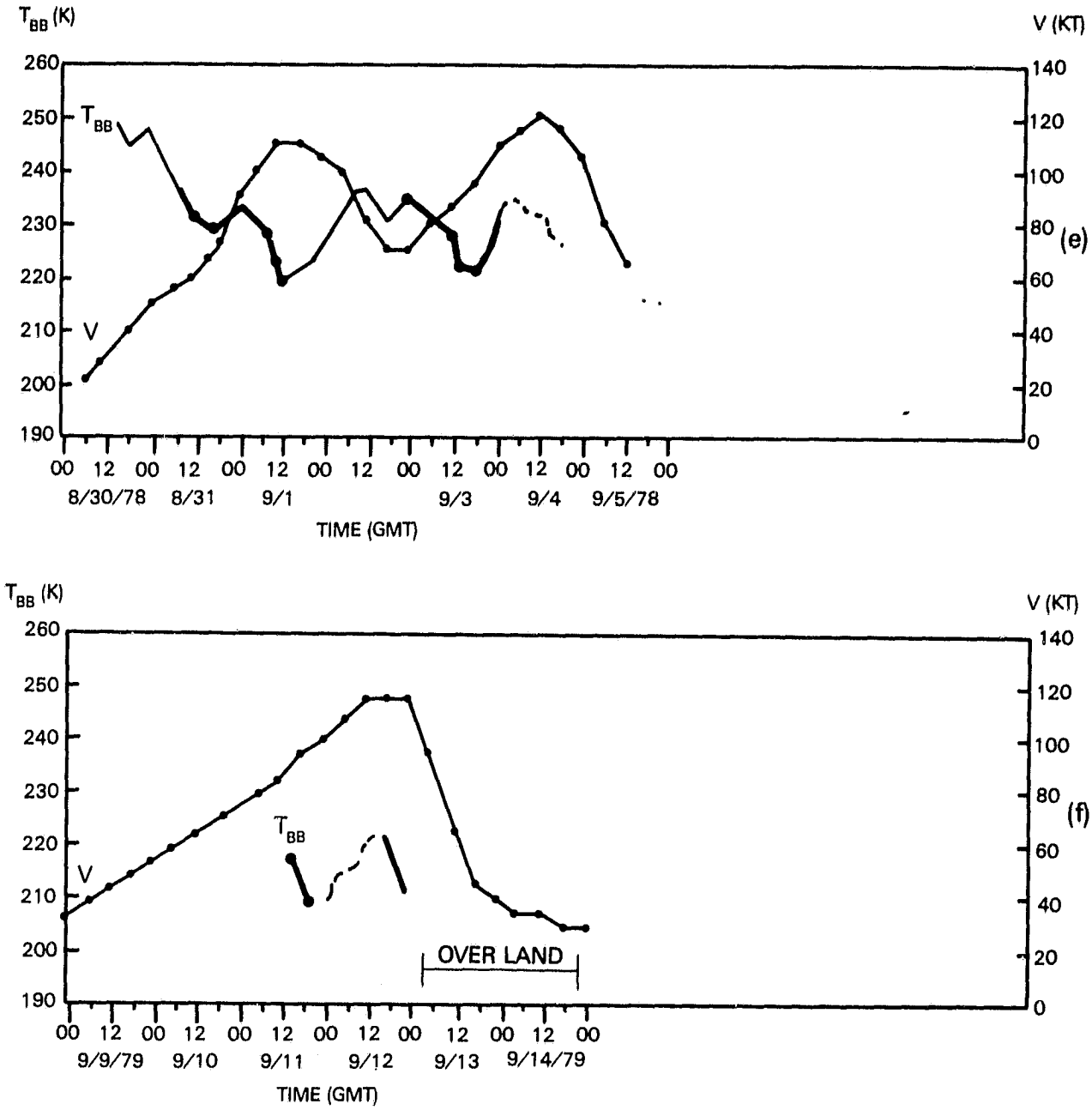

Figure 10. (e) Hurricane Ella, 1978. (f) Hurricane Frederic, 1979.